LBL-36455
UC-413

Lawrence Berkeley Laboratory
UNIVERSITY OF CALIFORNIA

Actinide Cation-Cation Complexes

N.J. Stoyer
(Ph.D. Thesis)

December 1994

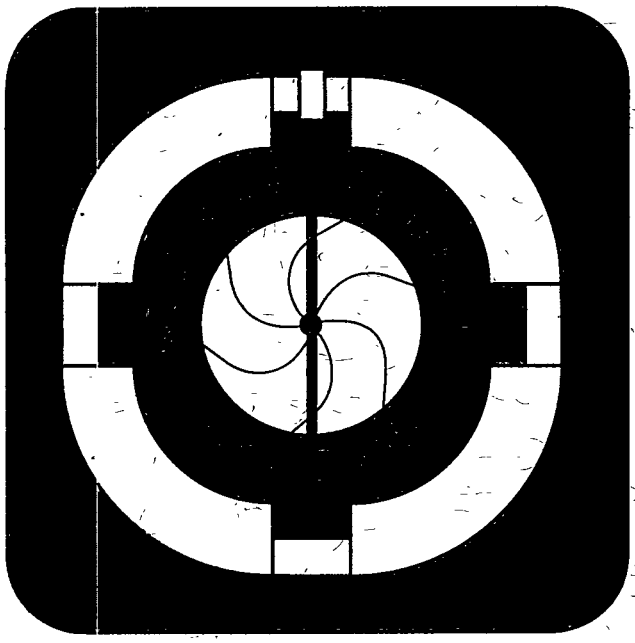

Prepared for the U.S. Department of Energy under Contract Number DE-AC03-76SF00098

LBL-36455
UC-413

Actinide Cation-Cation Complexes

Nancy Jane Stoyer
Ph.D. Thesis

Department of Chemistry
University of California, Berkeley

and

Nuclear Sciences Division
Lawrence Berkeley Laboratory
University of California
Berkeley, CA 94720

and

Glenn T. Seaborg Institute for Transactinium Science
Chemistry and Materials Science
Lawrence Livermore National Laboratory
Livermore, CA 94550

December 1994

This work was supported by the Director, Office of Energy Sciences, Chemical Sciences Division, of the U.S. Department of Energy under Contract No. DE-AC03-76SF00098; the U.S. Department of Energy through the Glenn T. Seaborg Institute for Transactinium Science at Lawrence Livermore National Laboratory under Contract No. W-7405-ENG-48; and the U.S. Department of Education Fellowship Grant No. P200A10143.

Abstract

ACTINIDE CATION-CATION COMPLEXES

by

Nancy Jane Stoyer

Doctor of Philosophy in Chemistry

University of California at Berkeley

Professor Darleane C. Hoffman, Chair

The +5 oxidation state of U, Np, Pu, and Am is a linear dioxo cation (AnO_2^+) with a formal charge of +1. These cations form complexes with a variety of other cations, including actinide cations. Other oxidation states of actinides do not form these cation-cation complexes with any cation other than AnO_2^+; therefore, cation-cation complexes indicate something unique about the chemistry of AnO_2^+ cations compared to the chemistry of actinide cations in general. The first cation-cation complex, $NpO_2^+ \cdot UO_2^{2+}$, was reported by Sullivan, Hindman, and Zielen in 1961. Of the four actinides that form AnO_2^+ species, the cation-cation complexes of NpO_2^+ have been studied most extensively while the other actinides have not. The only PuO_2^+ cation-cation complexes that have been studied are with Fe^{3+} and Cr^{3+} and neither one has had its equilibrium constant measured. Actinides have small molar absorptivities and cation-cation complexes have small equilibrium constants; therefore, to overcome these obstacles a sensitive technique is required. Spectroscopic techniques are used most often to study cation-cation complexes. A relatively new absorption spectroscopy technique called Laser-Induced Photacoustic Spectroscopy which is two to three orders of magnitude more sensitive than conventional absorption spectroscopy was used in this research. The equilibrium constants for the complexes $NpO_2^+ \cdot UO_2^{2+}$, $NpO_2^+ \cdot Th^{4+}$, $PuO_2^+ \cdot UO_2^{2+}$, and $PuO_2^+ \cdot Th^{4+}$, determined at an ionic strength of 6 M using LIPAS are: 2.4 ± 0.2, 1.8 ± 0.9, 2.2 ± 1.5, and ≈ 0.8 M^{-1}, respectively.

Dedication

To
Bobbi Anne McConaghy Shock
for
the life she lived,
the person she was,
and
the memories that remain.

To
Mark Alan Stoyer
because he is my
friend,
husband,
lover,
confidant,
and
greatest supporter.

Acknowledgements

First, I would like to thank those organizations that provided funding for my graduate research, namely the Director, Office of Basic Energy Sciences, Chemical Sciences Division of the U.S. Department of Energy under Contract No. DE-AC03-76SF00098; the U.S. Department of Energy through the Glenn T. Seaborg Institute for Transactinium Science at Lawrence Livermore National Laboratory under Contract No. W-7405-ENG-48; and the Department of Education. The Heavy Element Production Facility at ORNL produced the ^{242}Pu used in this research.

I would like to thank Dr. Kenton J. Moody and Dr. Mark A. Stoyer for the dissolution and purification of the ^{237}Np used in these experiments.

I would like to thank Dr. Darleane C. Hoffman, my Research Advisor. She provided me with an opportunity to study and learn many things during my time as a graduate student.

I would like to thank the past and present members of SHEIKS, too many to attempt to name; besides, they know who they are.

The Actinide Geochemistry Group at LBL (formerly under Dr. Heino Nitsche, presently under Dr. Dave Hobart), especially Kevin Roberts and Raymond Gatti, were very helpful with the ^{242}Pu purification and oxidation state changes.

The Lawrence Berkeley Laboratory 88-inch Cyclotron and its staff provided many interesting days, evenings, and nights, not to mention a rounded graduate student experience, while working on the labor intensive on-line experiments of my colleagues.

I would like to thank those out at LLNL who helped me with my thesis research. Dr. Robert Silva was my initial LLNL sponsor and introduced me to the subject of cation-cation complexes. Dr. Rick Russo, Dr. Greg Klunder, and Dr. David Wruck were a tremendous help with the LIPAS system. The Shape Isomer group gave me not only their friendship but also the use various printers and computers. Rich Torres, John Andrews, Leon Newton, Dave Tinoco, and Ron Lougheed were just a few of the many helpful people.

I want to thank the professors at Berkeley that have contributed to my tenure as

a graduate student, especially Dr. John Rasmussen and Dr. Stan Prussin. I would also like to thank those chemistry professors that encouraged me to go to graduate school while I was still an undergraduate at California State University, Stanislaus, especially Dr. Michael J. Perona, Dr. James E. Byrd, Dr. Hobart Hamilton, and Dr. Evan M. Thompson.

I would like to thank my family and friends for all of their support and encouragement, especially Mark, Ernest, Verla, Pam, Dennis, Teri, Jeff, Tami, Dustin, Blake, Doug, Kathy, Michelle, Tom, Cathy, Kevin, Amy, Holly, Don, Leslie, Ryan, Erin, Laura, Bill, Melissa, Jason, Heather, Darin, Sandy, Mike, Robert, Marcus, Mari, Jo, Christina, Erik, Lyn, Dorothy, Dale, Janice, Fran, Len, Rachel, Elizabeth, Faye, Bing, John, Chris, Cal, Ann, Jeff, Phil (thanks for all of the help with the bias box), Susi, Yves, Rebecca, Dean, and I-wen.

Contents

List of Figures

List of Tables

Chapter 1

Introduction

1.1 General Background

By 1940, all but four of the elements through uranium had been discovered. The four heaviest elements, actinium, thorium, protactinium, and uranium, were placed in the periodic table at the bottom of groups 3, 4, 5, and 6, respectively. Their chemical properties suggested such placement was correct. With the discovery and elucidation of the chemical properties of neptunium and plutonium, it became apparent that placement in groups 7 and 8, as would be suggested for these next heaviest elements, was not warranted. Neptunium and plutonium behaved much more like uranium than the group 7 and 8 elements rhenium and osmium. In 1944, G. T. Seaborg [1] suggested the placement of actinium through the as yet undiscovered element 103 in a $5f$ series analogous to the $4f$ lanthanide series. Currently, these elements are now placed there in the periodic table as an actinide series. This placement indicated that the chemical properties of the actinides should be somewhat similar to actinium and

Table 1.1: Actinide oxidation states, where "M" is the most common oxidation state, "s" is able to be stabilized in aqueous solution, "u" is unstable (seen in solids or as transient species), and "c" is claimed but not independently substantiated. This information is from [2].

†	Element														
	Ac	Th	Pa	U	Np	Pu	Am	Cm	Bk	Cf	Es	Fm	Md	No	Lr
+1													c		
+2							u	u		u	u	s	s	M	
+3	M	u	u	s	s	s	M	M	M	M	M	M	M	s	M
+4		M	s	s	s	M	s	s	s	s	u	c			
+5			M	s	M	s	s	c		c					
+6				M	s	s	s	c							
+7					s	u	c								

†— Oxidation state

the homologous lanthanides.

Actinides exhibit an unusually broad range of oxidation states, from +2 to +7 [2] (and possibly +1 for Md [3]). The oxidation states for the actinide elements are shown in Table 1.1. With so many available oxidation states in aqueous solutions for some of the actinides, the chemistry is quite complex.

Actinides are also radioactive, collectively exhibiting all the major forms of radioactivity (α, β^-, β^+, electron capture, isomeric transition, and spontaneous fission). The fissionability and radioactive properties of the actinides make them useful for nuclear power, defense, space exploration, commercial, industrial and medical

applications.

Actinides and transactinides are also studied because of their placement in the periodic table, near the upper limit of nuclear stability and as the heaviest known element of a given group in the periodic table. Transactinium isotopes can provide many clues to nature's laws by their behavior. The chemical and physical properties of an element are determined by its electronic configuration. Deviations from the trend at the bottom of a group can be due to relativistic effects. These relativistic effects are caused by the increase in atomic number and increasing charge on the nucleus which more tightly binds the electrons. At a Z of about 90 the electron velocity can be about half the speed of light, definitely relativistic. The results [4] of this effect are (1) the contraction of the $s_{1/2}$ and $p_{1/2}$ orbitals, (2) the spin-orbit splitting, and (3) the expansion of the d and f orbitals due to the increased screening caused by (1). These effects can alter the order in which the orbitals are filled and the number and character of the valence electrons. Examination of the chemical and physical behavior of the heaviest elements can indicate whether the theoretical explanations and predictions of the electronic orbitals and their energy levels are consistent with reality and the magnitude of the effects.

During a study involving two actinides, NpO_2^+ and UO_2^{2+}, an interaction resulting in an actinide-actinide complex was found [5] as early as 1961. These cation-cation complexes have subsequently been found to form between an actinide in the +5

oxidation state and other cations. (See Chapter 2 for more information.) There are many elements that have an accessible +5 oxidation state; some form anionic species, others form intermediates or compounds, while the actinides tend to form linear dioxo cations. The elements with +5 oxidation states and the type of species they form are shown in Figure 1.1. Protactinium behaves more like Nb and Ta in many respects than like U, Np, and Pu [6]. Various formulas (depending upon the solution conditions) have been proposed as its +5 species, e.g., $PaOOH^{2+}$ [7, 8], $PaO(OH)_2^+$ [6, 9], PaO_2^+ (analogous to U, Np, Pu, and Am) [6, 9], and PaO^{3+} [6, 8]. The most recent reference [8] indicates the species is probably $PaOOH^{2+}$. Linear dioxo cations form the cation-cation complexes; hence, U, Np, Pu, and Am are the elements of interest because they are known to form the AnO_2^+ species.

1.2 Experimental Method

In this research, actinide cation-cation complexes involving NpO_2^+ and PuO_2^+ with Th^{4+} and UO_2^{2+} were studied using remote **L**aser-**I**nduced **P**hoto**A**coustic **S**pectroscopy (**LIPAS**). The studies were performed remotely using a fiber optic cable for light transmission to allow containment of the solutions of the radioactive elements within an inert atmosphere glove box. The species PuO_2^+ is oxygen sensitive so the inert atmosphere in the glove box extends its chemical life-time. LIPAS allowed examination of these radioactive solutions in a non-invasive and sensitive manner

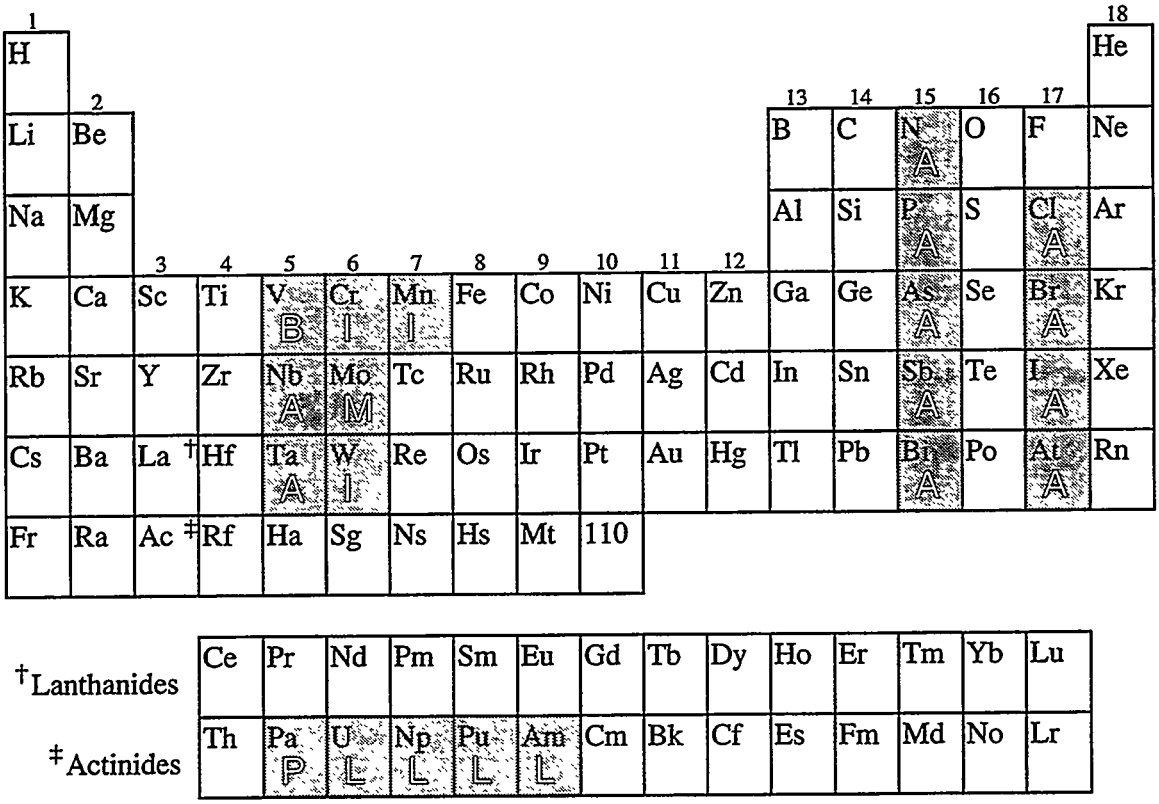

Figure 1.1: Elements with +5 oxidation state are shaded in grey. "A" indicates anionic species formation, "I" intermediate or solid compound formation, "B" bent dioxo-cation formation, "M" $Mo_2O_2^{2+}$ formation, "P" $PaOOH^{2+}$ formation, and "L" linear dioxo-cation formation. Data from [7].

without having to transport them to the measuring device. This avoids the potential for contamination during transport or measurement and also avoids exposure of the samples to air.

The formation of cation-cation complexes in non-complexing media extends our knowledge of ionic interactions in solution and our knowledge of AnO_2^+ behavior. Knowledge of the AnO_2^+ species is important because PuO_2^+ has been shown to be predominant under certain environmental conditions [10, 11].

The subject of cation-cation complexes, the studies so far, the indicated structures, and systematics will be discussed in Chapter 2. The theory, experimental setup, and limitations of LIPAS will be discussed in Chapter 3. The experimental procedures will be discussed in Chapter 4. The results obtained and a discussion of those results will be in Chapter 5. Finally, the conclusions that can be drawn from this research and some ideas on how it can be further explored will be discussed in Chapter 6.

Chapter 2

Cation-Cation Complexes

2.1 Literature

The first cation-cation complex discovered involved two actinides, neptunium (as NpO_2^+) and uranium (as UO_2^{2+}) [5]. The literature containing information on cation-cation complexes or intermediates involving two actinides is summarized in Table 2.1. Additionally, cation-cation complexes or intermediates involving an actinide and another element (typically a transition element) have been investigated; these studies are listed in Table 2.2.

The cation-cation complexation reaction is

$$AnO_2^+ + M^{n+} \rightleftharpoons AnO_2^+ \cdot M^{n+},$$

where AnO_2^+ is UO_2^+, NpO_2^+, PuO_2^+, or AmO_2^+, and M^{n+} is one of many ions (see Table 2.1 or Table 2.2 for some examples). The equilibrium constant, K_{eq}, is defined as

$$K_{eq} = \frac{[AnO_2^+ \cdot M^{n+}]}{[AnO_2^+] \cdot [M^{n+}]}, \tag{2.1}$$

Table 2.1: Actinide(V)·actinide cation-cation complexes.

	UO_2^+			NpO_2^+			PuO_2^+			AmO_2^+		
Ion	†	‡	ref.	†	‡	ref.	†	‡	ref.	†	‡	ref.
PuO_2^{2+}				c	s,r	[12]						
PuO_2^+	¿	k	[13]									
Pu^{4+}				¿	k	[14]						
Pu^{3+}	¿	k	[15]									
NpO_2^{2+}				3.0	s,e	[16]				0.095	s	[17]
				c	r	[12]						
NpO_2^+	¿	k	[18]	¿	k	[19]						
				0.82	s,r	[12]						
				1.41	s	[20]						
Np^{3+}				¿	k	[21]						
UO_2^{2+}	16.1	s,k	[22]	0.69	s,p	[5]				≈0.3	r	[12]
				3.7	s,e	[16]				0.35	s	[17]
				2.5	r	[12]						
				2.25	s	[20]						
UO_2^+				¿	k	[18]	¿	k	[13]			
Th^{4+}				c	s	[23]						
				c	r	[12]						

†K_{eq} (in M^{-1}) or the following codes are given:

c - complex formation indicated

? - complex formation questionable

¿ - intermediate indicated, questionable if cation-cation type

‡ Method(s) used is given using the following codes (explained in Section 2.1):

s - conventional absorption spectroscopy

p - potentiometric and proton spin relaxation

r - Raman spectroscopy

k - kinetic

e - electron paramagnetic resonance

Table 2.2: Actinide(V)-non-actinide cation-cation complexes.

	UO_2^+			NpO_2^+			PuO_2^+			AmO_2^+		
Ion	†	‡	ref.	†	‡	ref.	†	‡	ref.	†	‡	ref.
BiO^+				c	s	[23]						
				c	r	[12]						
Pb^{2+}				c	s	[23]						
				c	s,r	[12]						
Hg^{2+}				c	s	[23]						
Hg_2^{2+}				c	s	[23]						
Nd^{3+}				c	s,r	[12]						
Ce^{3+}	¿	k	[24]									
La^{3+}				?	s,r	[12]						
Sn^{3+}	c	s,k	[25]									
In^{3+}				c	s	[23]						
Ag^+				c	s,r	[12]						
Rh^{3+}				3.31	s,k	[26]						
				c	r	[12]						
Ga^{3+}				c	s	[23]						
Cu^{2+}				c	s,r	[12]						
Fe^{3+}				c	s	[23]	i	k	[27]			
				c	s,r	[12]						
Cr^{3+}	i	s,k	[28]	c	s	[23]	c	s	[29]			
				2.62	s	[30]						
				c	r	[12]						
VO^{2+}	i	k	[31]									
V^{3+}	¿	k	[32]									
Sc^{3+}				c	s	[23]						
Al^{3+}				c	s	[23]						
				c	s,r	[12]						

†K_{eq} (in M^{-1}) or the following codes are given:

c - complex formation indicated

? - complex formation questionable

i - intermediate indicated, cation-cation type

¿ - intermediate indicated, questionable if cation-cation type

‡ Method used is given using the following codes (explained in Section 2.1):

s - conventional absorption spectroscopy

r - Raman spectroscopy

k - kinetic

with units of M^{-1}. Neptunium is by far the most widely studied AnO_2^+ ion and plutonium is the only one that does not have a reported K_{eq}. Uranyl(VI) has a K_{eq} reported for cation-cation complexes with every known AnO_2^+ except PuO_2^+.

Cation-cation complexes have been studied using six different methods: (1) conventional absorption spectroscopy (CAS), (2) Raman spectroscopy, (3) potentiometry, (4) proton spin relaxation, (5) kinetics, and (6) electron paramagnetic resonance (EPR). Both CAS and Raman spectroscopy look for shifts in the normal uncomplexed wavelength spectrum to determine complex formation. In potentiometric studies the potential shift of the redox couple NpO_2^+-NpO_2^{2+} has been used to determine if complexation occurs; it was used in conjunction with CAS and proton spin relaxation [5]. Proton spin relaxation provides a way of measuring the effective concentration of a paramagnetic ion, i.e. NpO_2^+, and thus of measuring complex formation. Kinetic studies of a system (disproportionation or oxidation-reduction) where an AnO_2^+ species is either consumed or produced can provide information about the reaction mechanism involved. The mechanism can proceed through the formation of a cation-cation complex as an intermediate or product. EPR studies have been conducted to determine if the reaction is an abortive e^- transfer (detect free electron signal) or complexation (no free electron signal). Determinations of equilibrium constants are most frequently made using CAS, sometimes in combination with other methods.

2.2 Complex Structure

Because cation-cation complexes are, by definition, complexes involving two like-charged ions there is great interest in their structure. It has been noticed that cation-cation complexes have only been formed between AnO_2^+ and another cation, but not between AnO_2^{2+} and any cation other than AnO_2^+. The difference in the AnO_2^+ structure compared with the AnO_2^{2+} structure is expected to be responsible for complex formation, and perhaps there are other unique properties associated with this difference.

NpO_2^+ forms complexes with both Rh^{3+} and Cr^{3+}, which have different electronic structures. Murmann and Sullivan [26] pointed out that because both Rh^{3+} and Cr^{3+} form cation-cation complexes with similar equilibrium constants, there is not a strong dependence on electronic structure but rather on electrostatic interactions. Because Cr^{3+} exchanges its first coordination sphere slowly and the $NpO_2^+ \cdot Cr^{3+}$ complex is formed slowly, inner-sphere complexation is expected.

Eigen and Wilkins [33] proposed that complex formation proceeds by first forming an outer-sphere complex where the two species are separated by at least one water molecule and then, if the ligand is strong enough, the water is ejected and an inner-sphere complex is formed. Actinides form both inner-sphere and outer-sphere complexes.

Frolov and Rykov [34] suggested cation-cation complexes are not complexes but

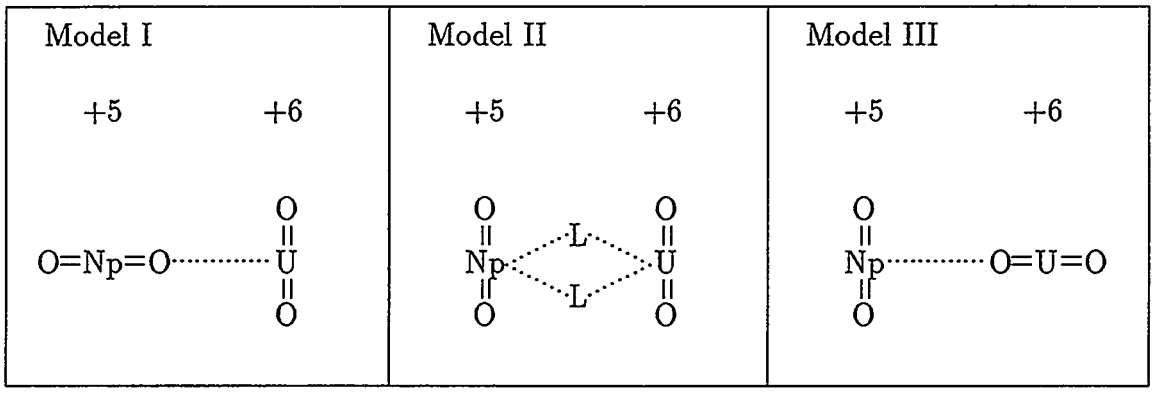

Figure 2.1: Cation-cation complex structure models. The dotted lines indicate the cation-cation complex forming bonds and "L" stands for bridging ligand. The models are discussed in the text.

rather abortive e^- transfers. Madic et al. [16] searched for e^- transfer evidence using EPR; however, the characteristic signal from a free electron was not seen. They further stated that the interactions between NpO_2^+ and NpO_2^{2+} or UO_2^{2+} were complexes because they followed the law of mass action.

There are three models for cation-cation complex structure. These models are shown in Fig. 2.1. Two of the models, Model I and Model III, show inner-sphere coordination; the two cations are "bonded" directly to each other. Model II shows outer-sphere coordination; the two cations are not "bonded" directly to each other but rather through another species called the bridging ligand.

Model I has been supported by Sullivan [23] and Vodovatov et al. [35, 36]. This model has an AnO_2^+ oxygen bonding in the ligand cation's equatorial plane. This model is consistent with shifts in AnO_2^+ vibrational modes in the infrared and visible

regions of the spectrum by complex formation and is consistent with very little, if any, effect on the ligand cation's vibrational modes. However, this model does not indicate why these complexes form with AnO_2^+ and not AnO_2^{2+}, unless, as suggested by Vodovatov et al. [35], the AnO_2^+ cation, in contrast to the AnO_2^{2+} cation, has a small negative charge concentrated on the oxygen atoms attached to it. Known complex structures for the actinides have bonding occurring through the central metal atom and not the axial oxygen atoms.

Model II has an outer-sphere complex formed where bridging ligands "bond" the two cations. This structure has been seen in other complexes, e.g. hydrolytic dimers of AnO_2^{2+} species where the bridging ligands are oxygen atoms of hydroxide groups. Studies of cation-cation complexes use an acidic non-complexing media where perchlorate ions and water are the available ligands. Perchlorate ions are weakly complexing ions and are not known to bind neighboring cations. Water has been reported to act as a bridging ligand in one case, the dimer $[UO_2(NO_3)_2(H_2O)]_2 \cdot 2C_3H_4N_2$ [37]. Because this model describes the formation of hydrolytic dimers of AnO_2^{2+} species, it does not provide an obvious reason for AnO_2^+ cations and not AnO_2^{2+} cations forming cation-cation complexes.

Model III is the only model with an apparent reason for AnO_2^+ forming cation-cation complexes and not AnO_2^{2+}. In this model the AnO_2^+ has the ligand cation in its equatorial plane forming an inner-sphere complex. The AnO_2^+ would form these

complexes because its hydration sphere is less ordered than the AnO_2^{2+} hydration sphere [39], although Vodovatov et al. [36] suggest that the AnO_2^+ might have a larger hydration shell than AnO_2^{2+} as a result of hydrogen bonding with the oxygen atoms on AnO_2^+. Vibrational frequency shifts and bond length changes can be accounted for using the inductive effect where the ligand cation "pulls" the electrons on the central atom in the AnO_2^+ cation which in turn affects the electrons around the oxygen. With such a small portion of the ligand cation complexed with the AnO_2^+ cation it is questionable whether or not changes in the ligand cation spectrum could be detected.

Models I and III both explain the experimental results; although, in a slightly different manner. The correct explanation is connected with the AnO_2^+ axial oxygen charge and hydration sphere.

There is debate about whether the cation-cation complex structure is inner or outer sphere. A study of the $NpO_2^+ \cdot UO_2^{2+}$ complex using wide-angle X-ray scattering was performed to look for evidence of ClO_4^- or H_2O acting as bridging ligands in an outer-sphere complex, or direct bonding through an axial oxygen atom of the AnO_2^+ species in an inner-sphere complex. The data were consistent with both interpretations [38]. Choppin [39] stated that negative entropies and enthalpies typically indicate solvent-separated (outer-sphere) complexes among the actinides. The thermodynamic data shown in Table 2.3 has negative enthalpies and entropies for four of the six complexes. This would suggest outer-sphere complexation. However,

Table 2.3: Thermodynamic data for cation-cation complex formation. The temperature coefficient method was used for ΔH and ΔS determinations.

Complex	ΔH, $\frac{\text{kJ}}{\text{mol}}$	ΔS, $\frac{\text{J}}{\text{mole·K}}$	ref.
$UO_2^+ \cdot UO_2^{2+}$	-7.9 ± 1.3	-4 ± 4	[22]
$NpO_2^+ \cdot Cr^{3+}$	-13.8 ± 2.5	-37.7 ± 7.9	[30]
$NpO_2^+ \cdot Rh^{3+}$	-15.1 ± 3.8	-42 ± 13	[26]
$NpO_2^+ \cdot UO_2^{2+}$	-12.0 ± 1.7	-34 ± 6	[20]
$NpO_2^+ \cdot NpO_2^+$	≈ 0	3 ± 2	[20]
$NpO_2^+ \cdot NpO_2^{2+}$	≈ 0	≈ 9	[16]

Stout, et al. [20] suggest that if a complex has inner-sphere coordination, negative entropies and enthalpies could be interpreted as meaning that the inner-sphere complex is more hydrated than the two reactants separately indicating greater solvent molecule net ordering around the complex.

2.3 Systematics

General observations of cation-cation complex formation indicate that they occur mainly in solutions with high ionic strength, μ (typically 2 M or higher), do not have a formal charge greater than +6, are more stable in perchlorate media then nitrate media [16], and are more stable with UO_2^+ than with NpO_2^+. The K_{eq}'s determined for the cation-cation complexes are small, 0.095–16.0 M^{-1} for a solution with μ = 2–10 M. From the long list of species that form cation-cation complexes with

NpO_2^+, it appears that most multiply charged cations will complex with NpO_2^+.

Determination of systematics of cation-cation complexes is difficult with a small data set for which the parameters were not kept constant (i.e., μ, background electrolyte) in different studies. The literature data for K_{eq} and μ are shown in Table 2.4. Fig. 2.2a is a plot of K_{eq} for $NpO_2^+ \cdot UO_2^{2+}$ complex vs. μ; clearly K_{eq} shows an increase with increasing μ. Fig. 2.2b is a plot of K_{eq} for $NpO_2^+ \cdot M^{n+}$ complexes vs. the effective charge[a], n, of the ligand cation's central metal (μ varies from 6–8 M within the data set); K_{eq} also shows an increase with increasing n. Fig. 2.2c is a plot of K_{eq} for $AnO_2^+ \cdot UO_2^{2+}$ complexes vs. atomic number, Z, (μ varies from 2–4.8 M within the data set); $\log(K_{eq})$ decreases with an increase in Z. See Section 6.1 for the discussion on the systematics of cation-cation complexes (results from this thesis will be included there).

[a]Effective charge, n, is a measure of the complexing strength of the cation. It is identical to formal charge for monatomic ions while for polyatomic ions it is an empirically determined number assuming ligands bind with the central metal atom; this number indicates the size of the apparent charge on the central metal atom influencing the complexation. Because the complexing strength of AnO_2^{2+} is greater than An^{3+}, hence n should be larger than 3. A value of 3.3 has been measured. The complexing strength of AnO_2^+ is smaller than An^{3+}, hence n should be less than 3. A value of 2.3 has been measured. See [39] for these results and further explanations.

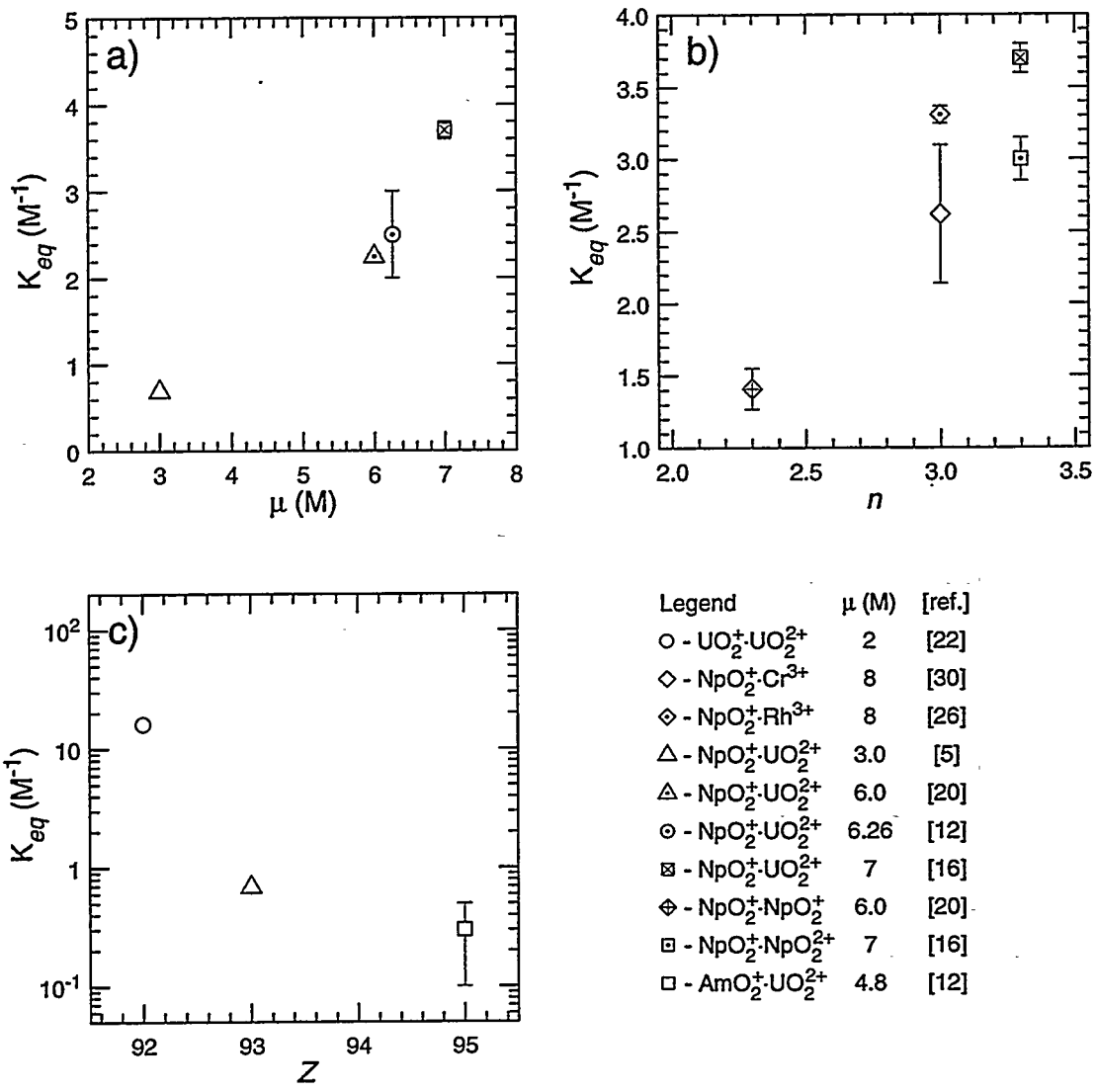

Figure 2.2: Systematics for cation-cation complexes. The data are from Table 2.4; a) K_{eq} for $NpO_2^+ \cdot UO_2^{2+}$ vs. μ; b) K_{eq} for $NpO_2^+ \cdot M^{n+}$ vs. n (effective charge) at approximately constant μ (6–8 M); and c) K_{eq} for $AnO_2^+ \cdot UO_2^{2+}$ vs. Z (atomic number) at approximately constant μ (2–4.8 M).

Table 2.4: Data on K_{eq} and μ for cation-cation complexes.

Cation	AnO_2^+								
	UO_2^+			NpO_2^+			AmO_2^+		
	K_{eq}, M^{-1}	μ, M	ref.	K_{eq}, M^{-1}	μ, M	ref.	K_{eq}, M^{-1}	μ, M	ref.
Cr^{3+}				2.62 ± 0.48	8	[30]			
Rh^{3+}				3.31 ± 0.06	8	[26]			
UO_2^{2+}	16.1 ± 0.5	2	[22]	0.69 ± 0.01	3.0	[5]	≈ 0.3	4.8	[12]
				2.25 ± 0.03	6.0	[20]	0.35 ± 0.06	10	[17]
				2.5 ± 0.5	6.26	[12]			
				3.7 ± 0.1	7	[16]			
NpO_2^+				0.82 ± 0.05	4.26	[12]			
				1.41 ± 0.14	6.0	[20]			
NpO_2^{2+}				3.0 ± 0.15	7	[16]	0.095 ± 0.030	10	[17]

Chapter 3

Laser-Induced Photoacoustic Spectroscopy

LIPAS is an absorption spectroscopy technique utilizing photoacoustics in which molecules in a solution are excited by the incident light or photons. Most of these molecules de-excite radiationlessly and release energy as heat. This released heat generates a sudden liquid expansion which causes an acoustic wave. These waves can be detected by a microphone or piezoelectric transducer (PZT). The amplitude of the acoustic wave is directly proportional to the strength of the absorption.

3.1 Applicability

LIPAS is similar to CAS, a widely used analytical method. Both depend upon photon interactions with the electrons around an atom or molecule and both generate similar spectra (see Fig. 3.1). The sensitivity of LIPAS is about two or three orders of magnitude greater than CAS. In Fig. 3.1a, the tiny bump at 616.0 nm in the main

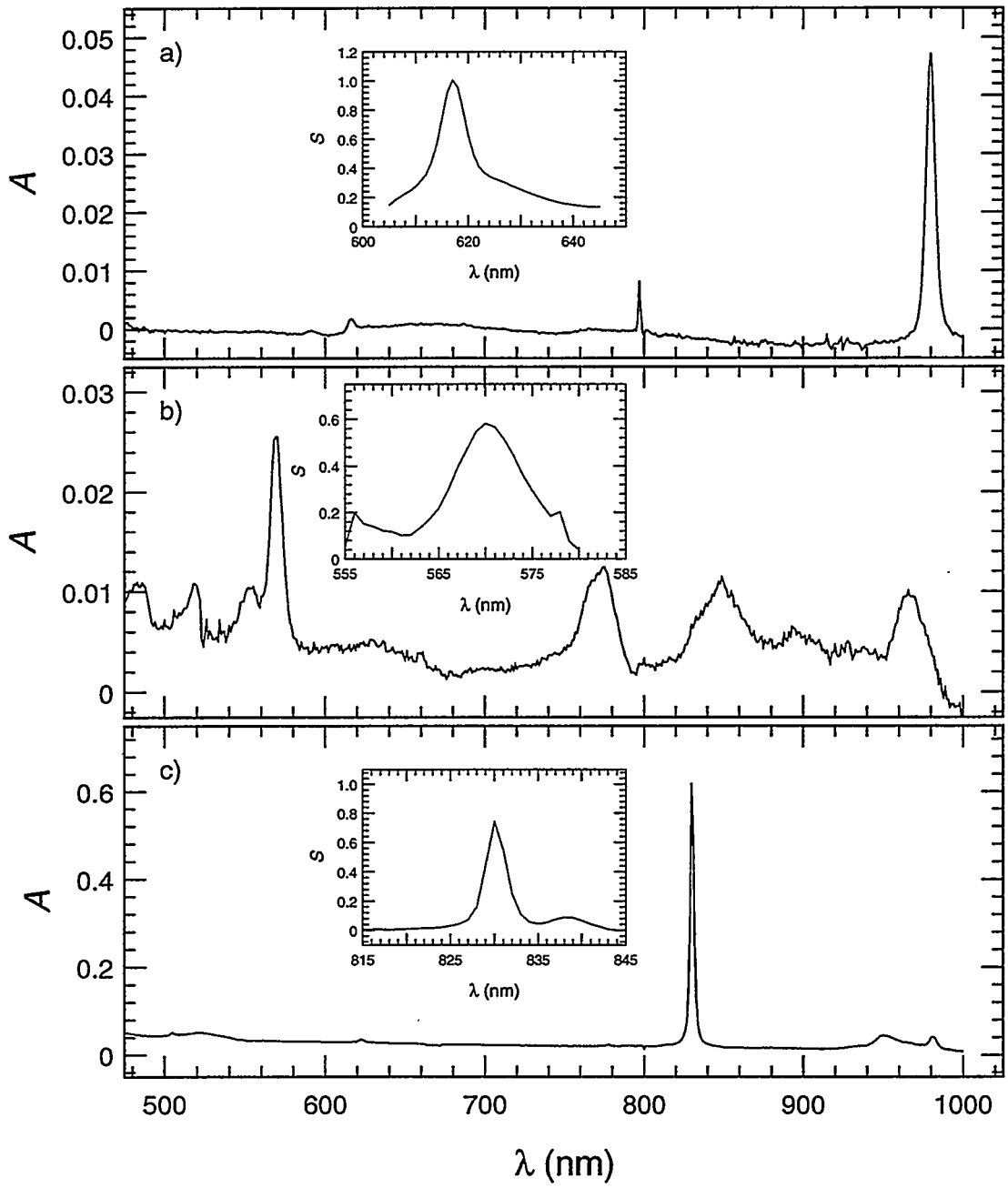

Figure 3.1: Comparison between LIPAS and CAS. Spectra are compared for a) NpO_2^+, b) PuO_2^+, and c) PuO_2^{2+}. The main spectra were taken using CAS (Guided Wave spectrometer) and the expanded inset spectra were taken using LIPAS. The concentration of the species of interest for the CAS spectra and LIPAS spectra are: a) 0.248 and 0.198 mM; b) 0.70 and 0.08 mM; and c) 0.70 and 0.08 mM, respectively. Note the different scales for the abscissas of the inset spectra and all ordinates. A is defined by Eq. 3.3 and is dimensionless. S is defined by Eq. 3.8 and is dimensionless.

spectrum taken using a CAS system is for a 0.248 mM NpO_2^+ solution; it has an absorbance of a little less than 0.002 (see Eq.3.3). The expanded inset spectrum taken using a LIPAS system is for a 0.198 mM NpO_2^+ solution (note that it is the 616.0 nm peak again); it has a normalized photoacoustic signal of about 1 (see Eq.3.8). The signal from the LIPAS system is greater than 500 times the CAS signal. The noise of the CAS system is about 3% of the peak mentioned above, while the noise of the LIPAS system is about 1% of the peak. The LIPAS system is not only much more sensitive but also has lower noise.

Absorption spectroscopy is a useful analytical tool because of Beer's law. The intensity, I, of light after passing through a sample is given by

$$I = I_0 e^{-\alpha bc}, \tag{3.1}$$

where I_0 is the initial intensity of light, α is a constant of proportionality, b is the path length, and c is the concentration of absorbing species. Eq. 3.1 can be rearranged to form

$$\ln\left(\frac{I_0}{I}\right) = \alpha bc, \tag{3.2}$$

after taking the natural logarithm. The absorbance of a solution, A, is defined by

$$A = \log\left(\frac{I_0}{I}\right), \tag{3.3}$$

which is dimensionless. Converting the natural logarithm in Eq. 3.2 to base 10 and

substituting it in Eq. 3.3 results in the well known form of Beer's law:

$$A = \varepsilon bc, \tag{3.4}$$

where $\varepsilon = \frac{\alpha}{\ln 10}$. It simply states that a linear relationship exists between the solution absorbance and the absorbing species concentration. Because some variables are functions of wavelength (e.g. A and ε), the variable with a superscript λ will be used as notation to emphasize this relationship (e.g. A^λ and ε^λ).

Beer's law can also be applied to multi-component systems and is stated as,

$$A^\lambda_{total} = A^\lambda_1 + A^\lambda_2 + \cdots + A^\lambda_n = \varepsilon^\lambda_1 bc_1 + \varepsilon^\lambda_2 bc_2 + \cdots + \varepsilon^\lambda_n bc_n,$$

where the subscripts 1, 2, ..., n refer to the different absorbing species. There are, of course, limitations to Beer's law; the solutions need to be dilute, component reactions need to be included, and monochromatic light needs to be used. Consequently, ε^λ is for a specific species, at a specific wavelength, valid for a certain concentration range.

Beer's law can be simplified using the expansion for $\ln x$ of

$$\ln x = (x-1) - \frac{(x-1)^2}{2} + \frac{(x-1)^3}{3} + \ldots, \tag{3.5}$$

for the interval $0 < x \leq 2$. Assuming x is close to 1, the first term can be used to approximate $\ln x$. Substituting $x = \frac{I}{I_0}$ in Eq. 3.5, truncated at the first term, and multiplying both sides by -1 gives

$$\ln\left(\frac{I_0}{I}\right) \approx \frac{I_0 - I}{I_0} = \frac{\Delta I}{I_0}, \tag{3.6}$$

ΔI is very small if x is close to 1. Converting the natural logarithm in Eq. 3.6 to base 10 gives

$$A = \log\left(\frac{I_0}{I}\right) = \varepsilon bc \approx \frac{1}{\ln 10}\frac{\Delta I}{I_0}, \tag{3.7}$$

for $\frac{I_0}{I}$ close to 1. LIPAS also shows a linear relationship between its signal and the concentration of the absorbing species analogous to Beer's law for conventional absorption spectroscopy. This analogous equation is

$$S^\lambda = \frac{H^\lambda}{E^\lambda} = Kc\Sigma^\lambda = c\mathcal{K}^\lambda, \tag{3.8}$$

where S^λ is the normalized photoacoustic signal at λ (similar to A), H^λ is the photoacoustic signal at λ resulting from the absorbed light (ΔI measurement), E^λ is the laser beam power (I) at λ which is used to approximate I_0 because $\frac{I_0}{I}$ is close to 1, K is a constant accounting for geometric factors and response factors for the photoacoustic signal detector and laser-beam power detector which is constant for the detector system, c is the absorbing species concentration, Σ^λ is analogous to ε at λ, and $\mathcal{K}^\lambda = K\Sigma^\lambda$. This simplification requires the amount of light absorbed to be very small and places even more stringent limits on the concentration range for the absorbing species. The term "photoacoustic signal" will be used in Chapters 4–6 to denote normalized photoacoustic signal. LIPAS spectra for NpO_2^+, PuO_2^+, and PuO_2^{2+} standards, and their corresponding "Beer's law" graphs for the peak, are shown in Figs. 3.2–3.4, respectively.

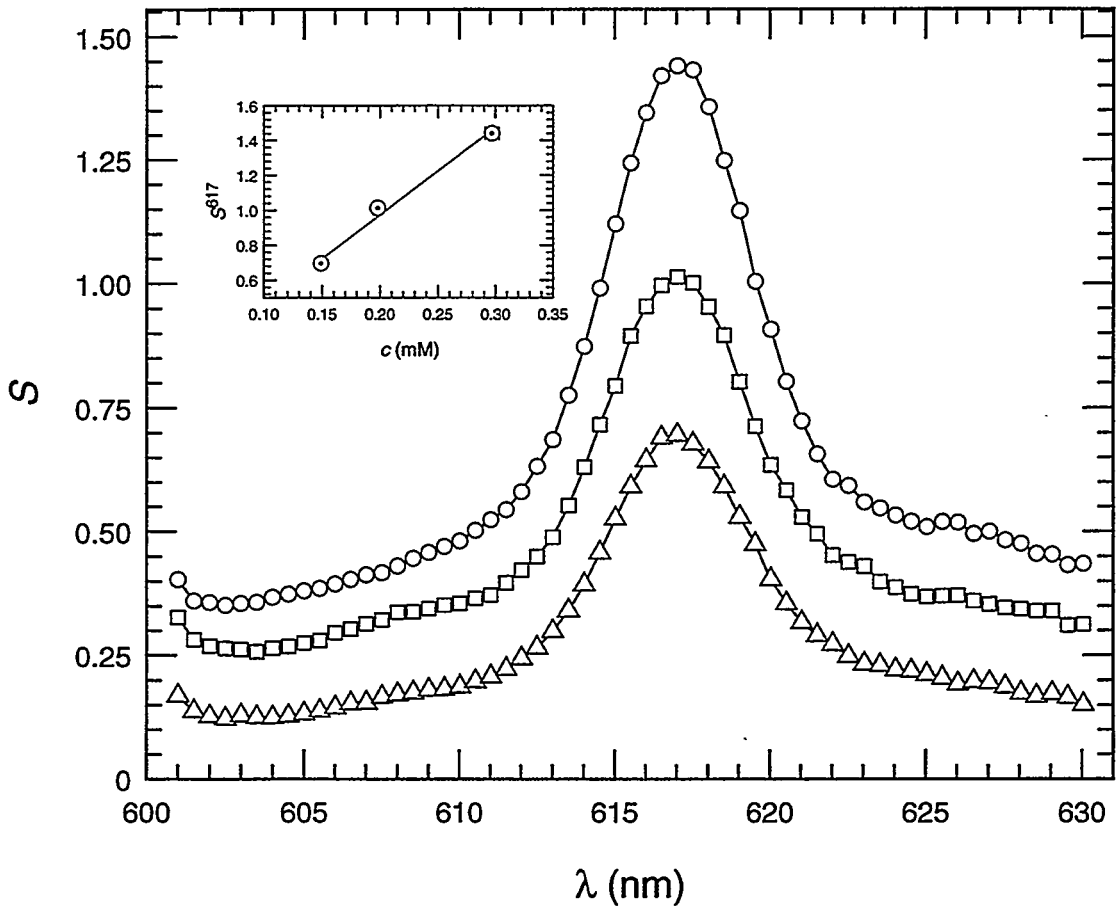

Figure 3.2: LIPAS spectra and Beer's law curve for NpO_2^+. The NpO_2^+ concentrations shown by the spectra are 0.297 mM for the circles, 0.198 mM for the squares, and 0.149 mM for the triangles, with lines joining the data points. The inset graph is the Beer's law plot for these spectra at 617 nm with a weighted least squares fit. Error bars for the points are shown only where they are larger than the symbol.

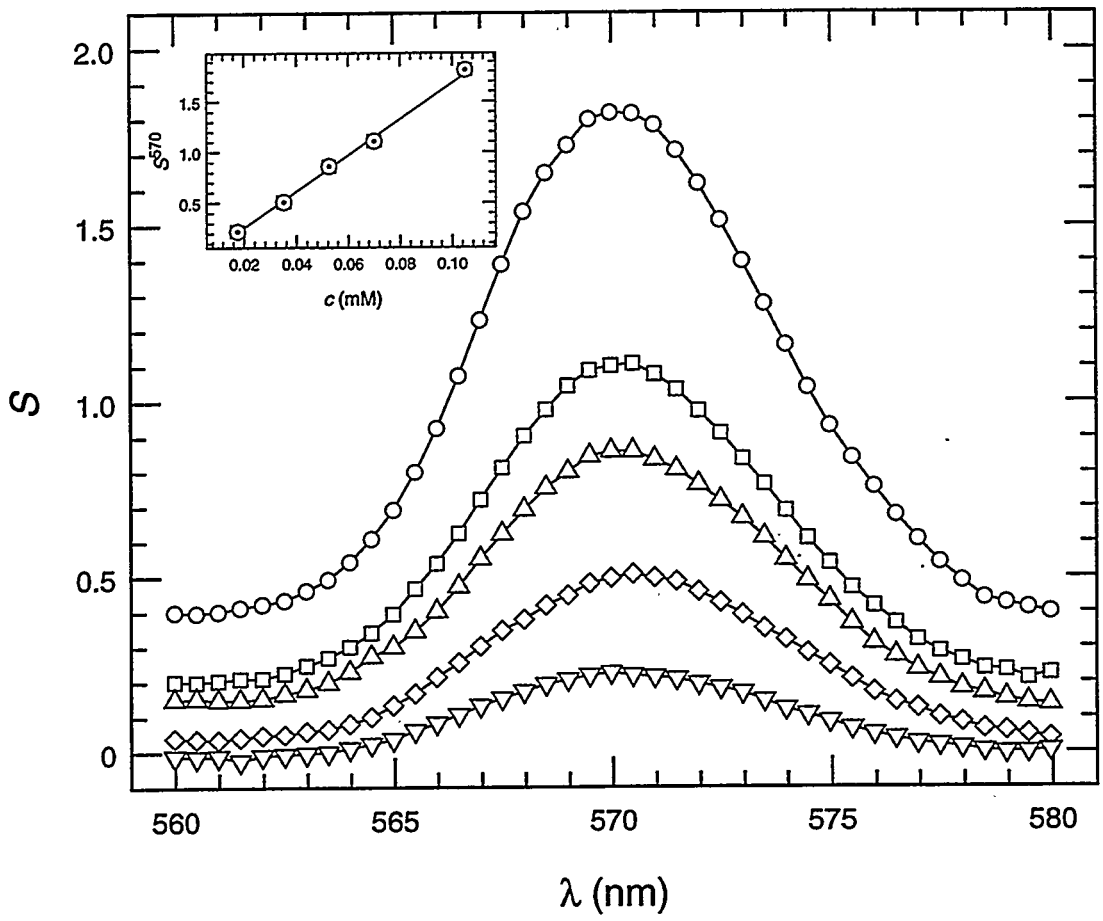

Figure 3.3: LIPAS spectra and Beer's law curve for PuO_2^+. The PuO_2^+ concentrations shown by the spectra are 0.105 mM for the circles, 0.070 mM for the squares, 0.052 mM for the point up triangles, 0.035 mM for the diamonds, and 0.018 mM for the point down triangles, with lines joining the data points. The inset graph is the Beer's law plot for these spectra at 570 nm with a weighted least squares fit. Error bars for the points are shown only where they are larger than the symbol.

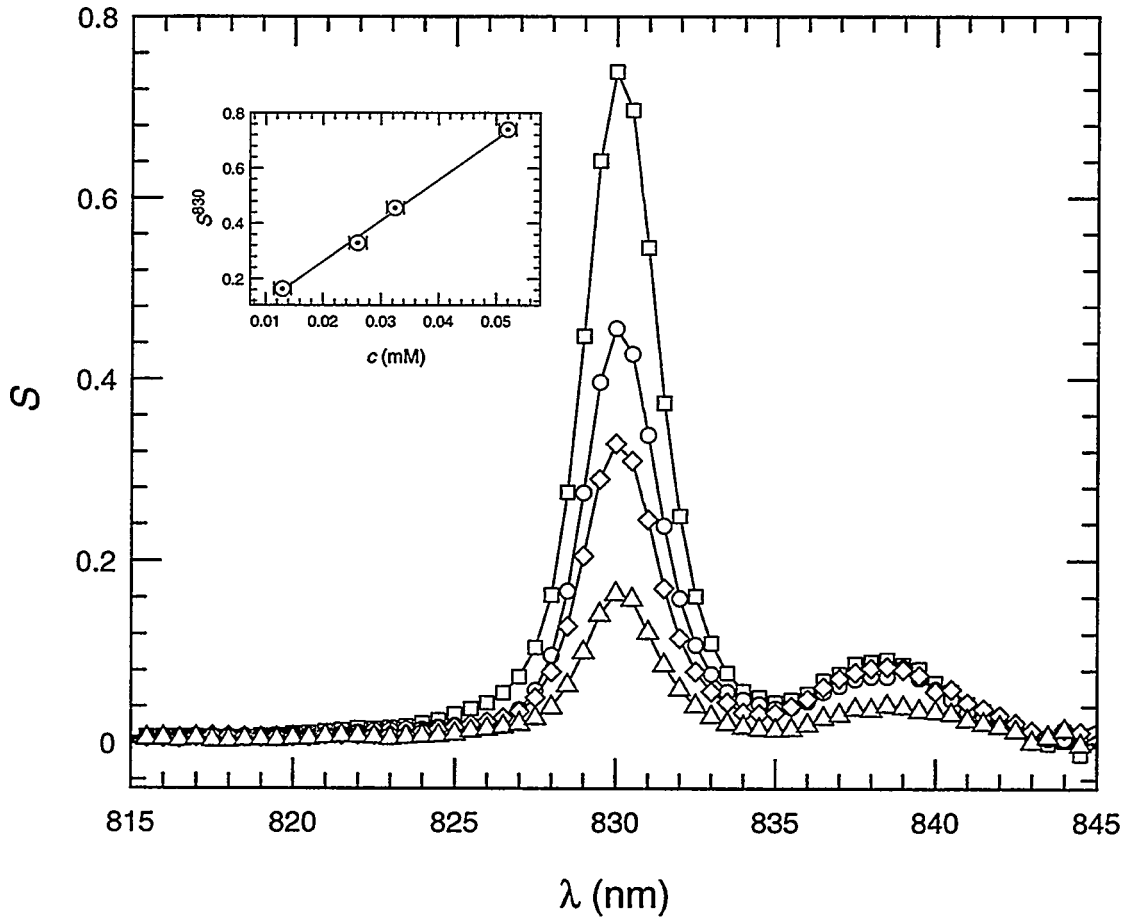

Figure 3.4: LIPAS spectra and Beer's law curve for PuO_2^{2+}. The PuO_2^{2+} concentrations shown by the spectra are 0.052 mM for the squares, 0.032 mM for the circles, 0.026 mM for the diamonds, and 0.013 mM for the triangles, with lines joining the data points. The inset graph is the Beer's law plot for these spectra at 830 nm with a weighted least squares fit. Error bars for the points are shown only where they are larger than the symbol.

3.2 System Description

The LIPAS system used for the present studies is very similar to the one described by Russo et al. [40]. For purposes of simplification the LIPAS system will be discussed in five steps; (1) generation of the laser beam, (2) focusing the laser bean onto the sample cuvette, (3) detection of the photoacoustic signal (using a PZT), (4) detection of the laser-beam power for normalization (using a photodiode, PD), and (5) acquisition of data. A LIPAS system block diagram is shown in Fig. 3.5.

The Nd:YAG laser (Spectra-Physics Quanta-Ray, DCR-3) produces a laser beam with a 1064 nm wavelength at 20 Hz. The laser beam then passes through non-linear optics consisting of an harmonic generator (Quanta-Ray, HG-2) and harmonic selector (Quanta-Ray,PHS-1). The harmonic generator can either allow the laser beam through unchanged, generate the 2^{nd} harmonic (halve its wavelength, 532 nm), or generate the 3^{rd} harmonic (355 nm). The harmonic selector extracts the required wavelength and directs it into the dye laser (Quanta-Ray, PDL-2). The dye laser, when coupled with the appropriate dye and pump wavelength, generates a laser beam which can be tuned over a wavelength range. Information on the commonly used laser dyes is contained in Table 3.1 and a graphical representation of the regions covered is shown in Fig. 3.6. A wavelength range is scanned using a computer interfaced stepping motor (Spectra-Physics Quanta-Ray, MCI) coupled to the grating inside the dye laser to produce spectra.

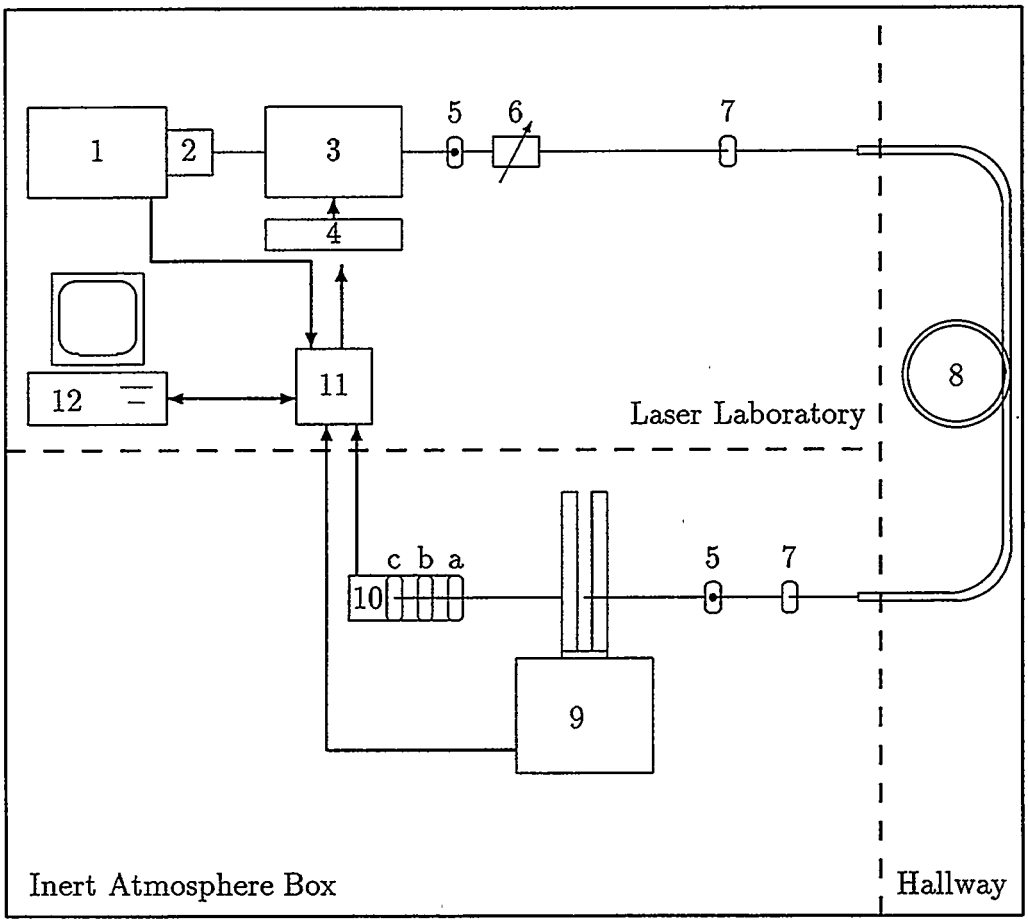

Figure 3.5: LIPAS system block diagram. The thick lines with arrows indicate cables for signal transmission in the arrow's direction; the thin lines indicate the laser beam path; and the dashed lines delineate the various component locations. The numbers identify the components as follows: (1) Nd:YAG Laser, (2) Non-linear optics, (3) Dye Laser, (4) Stepping motor, (5) Iris, (6) Variable Attenuator, (7) Lens, (8) Fiber optic cable, (9) PZT/Cuvette assembly, (10) PD assembly, a. Diffuser, b. Neutral density filters, c. Photodiode, (11) Electronics, (12) Computer. For more detail, see Section 3.2.

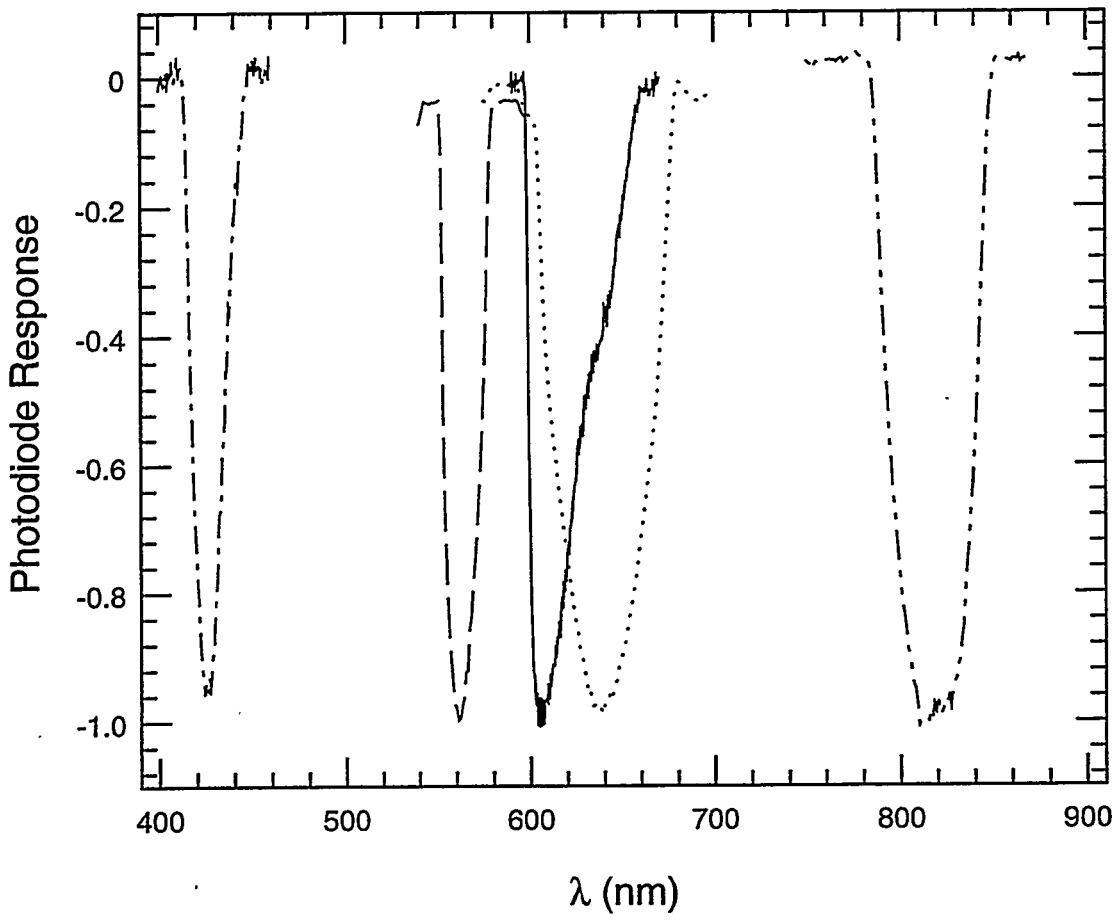

Figure 3.6: Dye gain curves for the laser dyes used. The normalized photodiode response as a function of wavelength for the dyes is shown. Dot-dashed line is for S420; dashed line is for R590; solid line is for DCM/R640 mixture; dotted line is for DCM; and the dot-dot-dashed line is for LDS821.

Table 3.1: Laser Dye information.

Dye†	Pump λ, nm	λ Range, nm	‡, mg/L	§, mg/L	Species	Half-life, h used	λ_{max}, nm
S420¶	355	415–445	250	55	UO_2^{2+}	0.25	428
R590£	532	552–580	115	17	PuO_2^+	300	560
DCM	532	605–672	175	24	NpO_2^+	> 300	640
LDS821 *	532	785–851	125	32.5	PuO_2^{2+}	> 40	815
mixture	532	600–650			NpO_2^+	> 300	605
DCM			91	12			
R640°			130	17			

† — All dyes purchased from Exciton.

§ — Oscillator Concentration.

‡ — Amplifier Concentration.

¶ — Stilbene 420, alternate name is Stilbene 3.

£ — Rhodamine 590, alternate name is Rhodamine 6G.

* — Alternate name is Styryl 9/9M.

° — Rhodamine 640, alternate name is Rhodamine 101.

The second step is focusing the laser beam onto the sample at its remote location via optical fibers. Before focusing the laser beam into the fiber, stray light is removed by adjusting the iris (Newport, ID-1.0). A variable attenuator (Newport, 935-5) adjusts the laser beam power sent to the remote part of the LIPAS system; typically, 40–60 mW is used for LIPAS measurements because the fiber face is damaged if the power exceeds 60 mW. Both lenses (Oriel, 41330, f=35 mm at the entrance in the laser laboratory and 41340, f=50 mm at the exit in the inert atmosphere box) focus the light to a point at the required locations. The fiber holder (Newport, RB-

MM2-2) at the input to the fiber optic cable (Fiberguide Industries, SFS-600-720B) is attached to a 3-D positioner (Newport, 460-XYZ Series) for fine adjustment of the fiber position with respect to the entering laser beam. The fiber optic cable allows the transport of the laser beam from the laser lab to an inert atmosphere glove box (MBraun, MB 150B-G-I(2500/780)) located in another room about 50 meters away. The fiber holder (Newport FP-2), iris, and lens at the remote end of the fiber are attached to a rail (Newport MRL-18) on an optical bread board (Newport SA-12 cut in half) together with the PZT/Cuvette assembly and PD assembly to insure co-linearity between these components.

The third step is detection of the photoacoustic signal. The PZT/Cuvette assembly performs this task. The PZT (Morgan Matoc, PZT5H) is a ceramic of a lead zirconate titanate material. A quartz cuvette (NSG Precision Cell, 29ES-10) contains the solution for measurement (maximum volume 1.3 ml). The laser beam is focused so that the focus point is within 1 cm of the cuvette. The cuvette has a 1 cm diameter by 1 cm long quartz rod is attached to the bottom with UV-curing epoxy to create a junction with less acoustic reflections. On the other end of the quartz rod a PZT is attached using silver epoxy. When the PZT and quartz rod were attached, two wires were attached to the PZT, one on each side, using silver epoxy. The PZT is enclosed in a metal "box" (the quartz rod is the feed through) for electrical noise minimization and is attached to a XYZ translator (Newport MT-XYZ). The two wires carrying the

signal are passed through the "box" using a lemo connector. A BNC cable (with lemo adapter) connects the "box" and the preamplifier (EG&G Ortec, 142C), located inside the inert atmosphere box, allowing pre-processing of the signal. The preamplifier output is connected to a BNC feedthrough to send the signal to the laser laboratory for data acquisition. The PZT signal is shown in Fig. 3.7.

The fourth step is detection of the laser power using the PD assembly to allow normalization. The first object that the laser beam encounters as it arrives at the PD assembly is the diffuser (Oriel, 48010). The diffuser spreads the laser beam out, thus reducing the power density. The neutral density filters (Oriel, 50284 and 50285) immediately behind the diffuser reduce the amount of light incident upon the PD (United Detector Technology, PIN-10DF) to levels that are within its linear response range. These filters reduce the laser power by a factor of 10^7. The diffuser and filters are attached to the PD housing by a lens holder (Newport, LH1-T) that has been bonded to the front of the housing using epoxy. The PD converts the light intensity into a voltage signal that is eventually sent through a BNC feedthrough to the laser laboratory for data acquisition.

The PD is +9 V reverse biased which improves its response. The bias box which provides the PD reverse bias was constructed at LLNL and the components are shown in Fig. 3.8. The signal from the PD for the same laser beam power (as measured in the laser lab) with and without the reverse bias is shown in Fig. 3.9. Reverse biasing

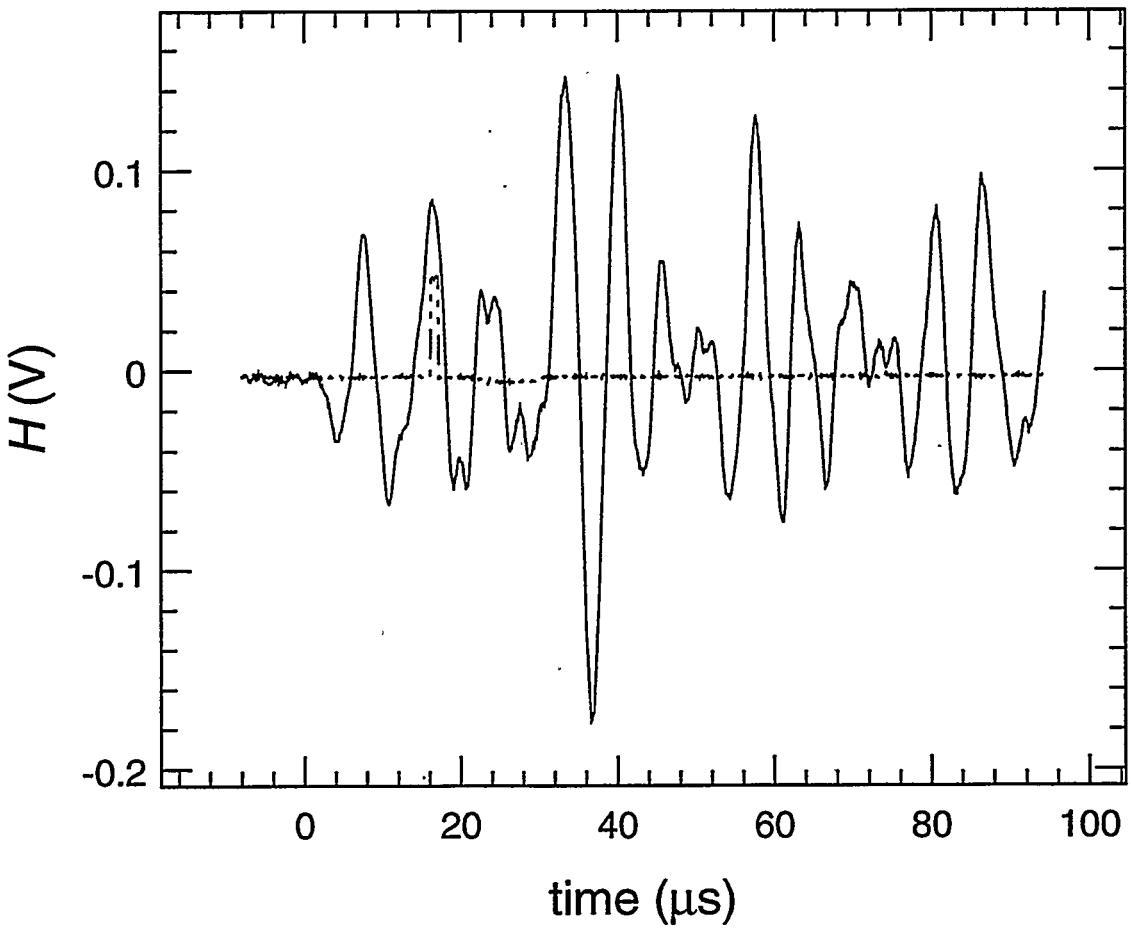

Figure 3.7: PZT signal as a function of time (solid line). The dashed line is the typical gate used for LIPAS measurements. The significance of the gate is discussed along with the data aquisition step. The shape of the PZT signal and choice of the gated peak is discussed is Section 3.3.1.

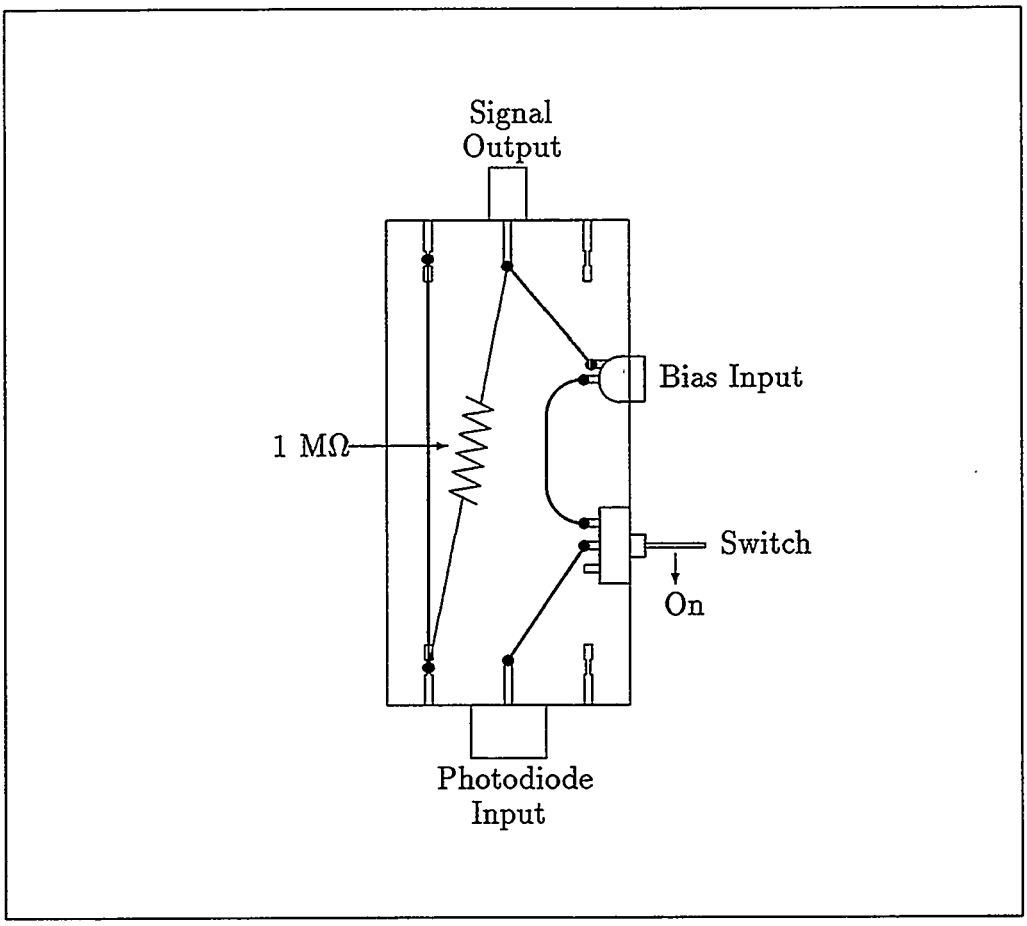

Figure 3.8: A schematic of the bias box. The bias input allows a 9 V battery to be connected using a lemo connector. The four posts with grooves are grounded. The connection at the signal output is a female BNC connector and a BNC cable is used to transmit the signal to the data aquisition system. The connection at the photodiode input is a male BNC connector to which the photodiode is attached (photodiode is received with a female BNC connector attached). A 1 MΩ resistor connects the signal output to ground. The heavy lines indicate wires connecting the various components.

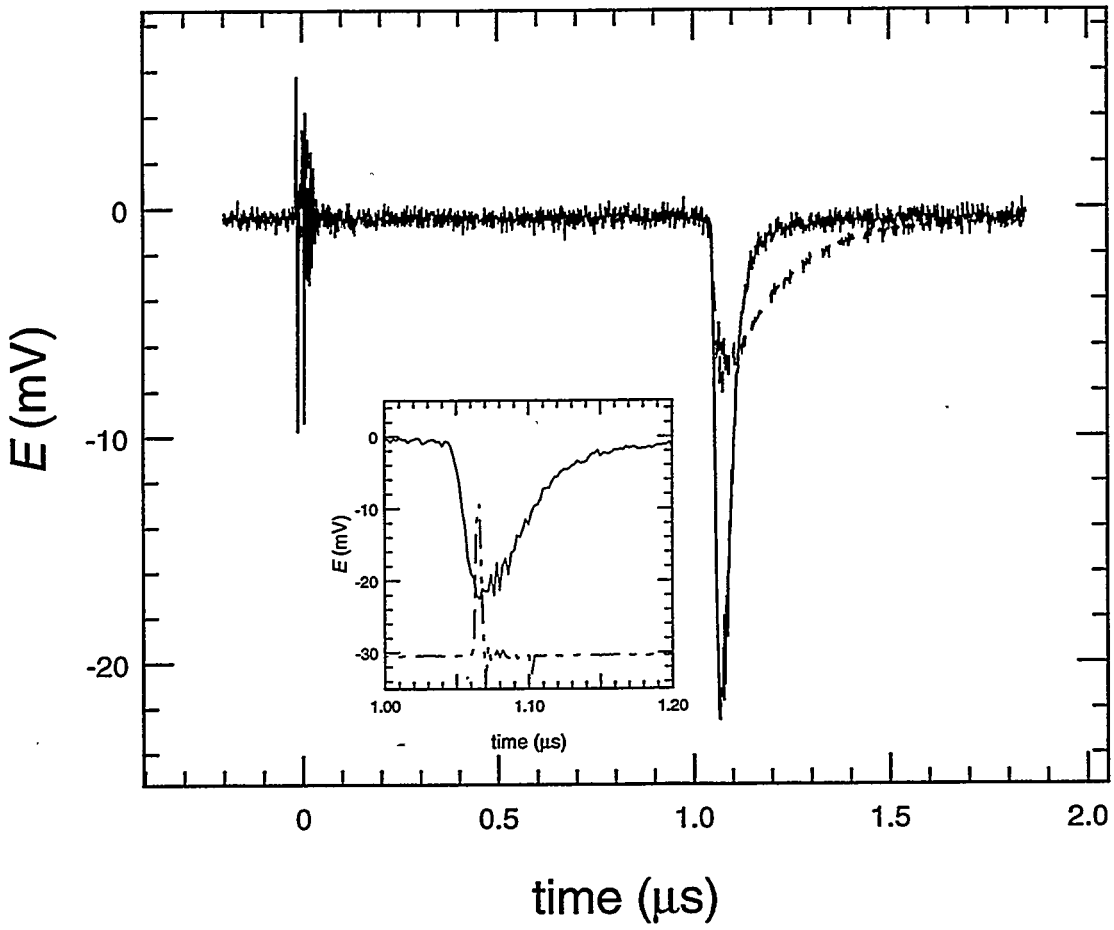

Figure 3.9: Photodiode signal as a function of time, with (solid) and without (dashed) 9 V reverse bias. The inset shows the typical gate (dashed line) for the reversed-bias photodiode signal used for LIPAS measurements. The significance of the gate is discussed along with the data aquisition step.

the PD was used because the signal is larger and has a faster response time.

The last step is the data acquisition. The signals from the laser (start time), PZT (photoacoustic signal), and PD (laser beam power) are processed by various electronics before being stored by the computer, which also controls the data acquisition. The timing of the various signals is shown in Fig. 3.10. The PD detects the laser beam which reaches the detector at the speed of light while the PZT detects the acoustic signal which reaches it at the speed of sound. This difference is seen in the positions of the gates for the two detectors. The laser pulses every 50 ms and has a pulse width of 4–7 ns depending on the wavelength of the pump laser. After preamplification, the PZT signal is amplified by a Ortec 570 amplifier. This amplifier has been modified so that all of the gains are reduced by a factor of 10, which is more useful for LIPAS. The amplifier output connects to the boxcar input (SRS Gated Integrator and Boxcar Averager); this boxcar generates the value H by averaging the signal over the gate width. All boxcars use the laser Q-Switch (Laser start pulse) output as the trigger source. The gate used for H is typically 17–19 μs after the trigger start and is about 900 ns wide (see Fig. 3.7). The H value is sent to channel 0 of the computer interface. Three other BNC outputs on the Boxcar allow the gate, signal, and trigger to be viewed using an oscilloscope.

The signal from the PD is sent to another boxcar to generate E, the averaged signal over the gate width. The gate typically used for E is 0.7–1 μs after the trigger

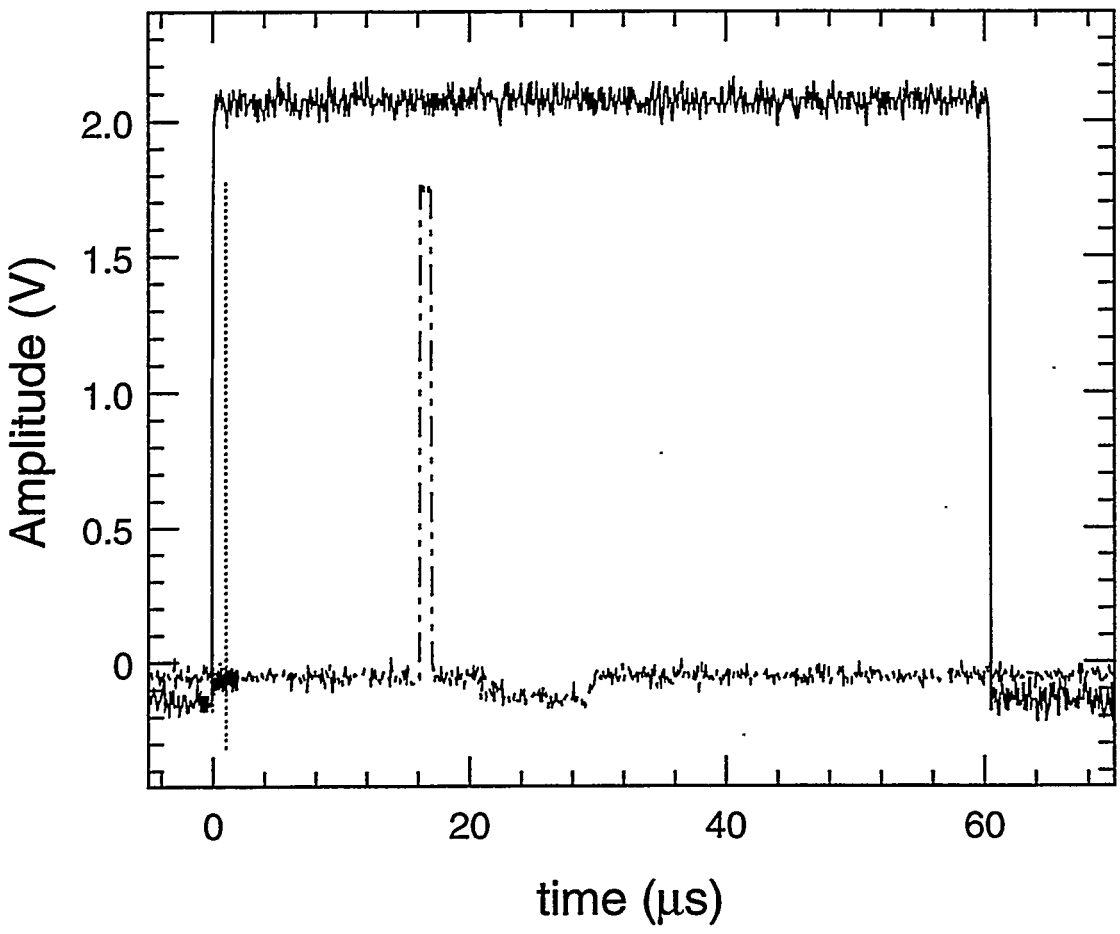

Figure 3.10: Timing diagram for the LIPAS system. The solid line is the trigger from the laser Q-Switch output. Although the gate generated is 60 μs wide, the laser pulse is actually 4–7 ns in duration and repeated every 50 ms. The dotted line is the gate for the PD signal which is 0.7–1 μs after the trigger and 6 ns wide. The dot-dot-dashed line is the gate for the PZT signal which is 17–19 μs after the trigger and 900 ns wide. The difference between the two gates is because the speed of light is faster than the speed of sound; the PD detects light and the PZT detects sound.

start and is about 6 ns wide (see Fig. 3.9). The E value is sent to channel 2 on the computer interface. The E value is typically monitored using a display module (SRS Power Meter and Display Module).

The computer is connected to the stepping motor of the dye laser to allow computer control of the wavelength via grating adjustments during data acquisition. The program used for control, LASER , was written by Richard Torres at Lawrence Livermore National Laboratory. The wavelength range, resolution, laser pulses per point, and number of scans can all be designated within the program, in addition to entering the pertinent hardware settings.

3.3 Limitations

LIPAS and other photoacoustic techniques have been described in the literature; however, to date no commercially built systems are marketed for LIPAS. There are a few other limitations on the LIPAS technique besides the Beer's law limitations mentioned previously (see Section 3.1).

3.3.1 Uniqueness

Each LIPAS system built at LLNL uses some purchased and some locally constructed equipment; therefore, each system is slightly different. The major differences have to do with photoacoustic detection and power normalization. The major contributions

to the uniqueness of each system are the cuvette acoustics, PZT response, and PD response.

The PZT generates a signal for every acoustic wave that reaches it; because acoustic waves are reflected by the various interfaces they encounter and these reflected waves can interfere constructively or destructively; therefore, the PZT signal is very complicated. The sound properties of the cuvette will vary with cell type (regular, semi-micro, and micro) and cell material; it may even vary from cell to cell for the same manufacturer and type. The solution contained within the cell will affect the acoustics and the liquid height will especially affect the sound reflections. The reason for using the peak at 17–19 μs after the laser trigger pulse for measurement is because this sound wave does not shift in time with the normal daily variations that occur when changing the sample in the cuvette; later peaks are shifted in time with minor solution height variations. Changing the solution type dramatically, e.g. from 6 M ionic strength solutions to 0.1 M ionic strength solutions, will shift all peaks in time. This is because the speed of sound is different in these solutions.

The response of the PZT will vary from one transducer to another. Tolerances are 20% of the values reported in the specifications for the PZT used. These differences are significant when comparing spectra taken using different LIPAS systems.

The PD response does not vary as much as some of the other components; however, reverse biasing does affect the response. The gate width used for measuring the PD

response should be set to optimize the stability of the signal. If using the reversed bias technique, one has to be aware that as a weak battery loses voltage the response will vary, and at some point the battery will cease to provide the reverse bias at all. The increase in signal intensity offsets the disadvantage of response variations provided the battery is changed before it discharges. A constant voltage source was tested to determine if it could be used in place of the battery. The signal shape from the PD using the constant voltage source was significantly different from the signal using the battery, hence the battery was kept.

3.3.2 Variability

Measurements of the same solution on different days can give slightly different spectra, usually minor height changes. The major contributions to the system variabilities are the laser stability and dye lifetimes.

The laser stability is greatly affected by room temperature. If the temperature exceeds approximately 80°F, the reproducibility of the laser-beam power on a pulse-to-pulse time scale, referred to as the stability of the laser, is greatly diminished and the spectra are too noisy to be useful. The laser must be run with an amplifier lamp energy greater than 30 J/pulse or a less stable beam is generated. Because the fiber optic cable can be damaged by excessive laser-beam power, it is sometimes necessary to attenuate the laser beam before it passes to the fiber optic cable.

The laser dyes producing the wavelength ranges have limited lifetimes. Most of the dyes used in this study had lifetimes on the order of 100 hours of use; other dyes can have lifetimes as short as an hour. As the laser dyes degrade during use, the amount of power is diminished, therefore less power is available for excitation of the solution, thereby increasing signal to noise. As a general rule, the dyes using a pump wavelength of 532 nm have longer lifetimes than those dyes using the 355 nm pump. The dyes using the 355 nm pump have 1 g of 1,4-diazobicyclo(2,2,2)octane per liter added to the dye solution to increase their lifetimes.

It is useful to have standards to monitor the LIPAS system before doing many measurements to insure that all parts of the system are functioning properly. Additionally, measuring all the solutions on the same day, including the solutions for the Beer's law curve, helps reproducibility. Cross calibration can be accomplished using a standard that has an absorbance peak very close to the species of interest provided the standard's molar absorptivity and concentration are well known and the species of interest has a well known molar absorptivity or concentration.

Amplified spontaneous emission (ASE) reduces laser efficiency and increases background noise. It is a broad-band spectral background from the dye fluorescence which exhibits laserlike properties. ASE is more prominent toward the edges of the dye gain curve where lasing efficiency is reduced. Because ASE can be absorbed by the sample producing a signal, it needs to be minimized. This can be accomplished by reduc-

ing the number of amplification steps within the dye laser; unfortunately, this also reduces the power available for sample excitation.

Once the LIPAS system is set-up for an experiment, it is best to disturb the apparatus as little as possible. Small changes in beam position relative to the cuvette can alter the acoustic pattern; thereby, altering the signal.

3.3.3 Design Constraints

The actual design of the LIPAS system used in this study limits the region of usefulness. Some of the major design constraints are the wavelength range and dynamic range.

The wavelength range available is determined by the laser dyes. The usable wavelength range is determined by the ability of the photodiode to detect light at that wavelength and by the ability of light at that wavelength to be transmitted through the cuvette and fiber optic cable. The item that imposes the most stringent limits is the laser dye. Laser dyes have usable regions on the order of a few nanometers to tens of nanometers. Because the extreme ends of the available wavelength range for the laser dye are subject to more variability, one should avoid working there. The wavelengths at which the laser dye produces the most power are best because there is proportionately less ASE, more power for excitation of the solution, and less fluctuation of power due to degradation of the dye.

The concentration range of the absorbing species for which one can measure a spectrum is limited by the maximum voltages that the electronics can accept (e.g. the boxcars used can accept signals with magnitudes of up to 2 V) and the noise within the system; therefore, only 1.5 to 2 orders of magnitude in species concentration are accessible. The neutral density filters in front of the PD adjust the maximum laser power that will elicit a linear response; however, with remote systems these are difficult to change.

3.3.4 Background

Occasional problems with spurious, as yet, unexplained noise in the instrument occur. This noise seems to be more prevalent between 9 a.m. and 5 p.m. when there is more activity within the building and has lasted for 20 minutes on occasion. This problem is referred to as breakdown and is evidenced by huge PZT signals.

One has also to be careful of background created by solution constituents. High ionic strength solutions have a higher background. ASE will create a higher background for high ionic strength solutions when the background electrolyte is excited by the ASE. Careful selection of the background electrolyte is necessary.

Species that have measurable ε at wavelengths away from characteristic peaks can pose a background problem when they are present at relatively high concentrations. Because LIPAS is a very sensitive method, all solution constituents except those whose

response is being measured should have no absorbance in the region being scanned. It is relatively easy to have a signal that is too large for the electronics to accept.

3.4 Justification

Although LIPAS has some limitations, its sensitivity and resolution capabilities make it an attractive instrument for the study of actinides. Because actinides typically have small molar absorptivities (see Table 3.2) and concentrations typically used are low (mM to μM), high sensitivity is needed; with two to three orders of magnitude more sensitivity than CAS, LIPAS can detect low concentrations of the actinides. The user can also select the resolution, with a commensurate increase in scan time, to allow the spectral features desired to be resolved. The remote LIPAS system allows measurements of solutions of radioactive samples to be made without removing them from the glove box. This eliminates the possibility of radioactive contamination of the laser and associated electronics due to sample spills; only the remote apparatus which is contained within the inert atmosphere box can be contaminated. In addition, the samples can be kept in a controlled atmosphere.

Table 3.2: Information on ε^{λ} for selected actinide species.

Species	λ, nm	ε^{λ}, $M^{-1}cm^{-1}$
UO_2^{2+}	415	8
NpO_2^{+}	616	23
PuO_2^{+}	569	17
PuO_2^{2+}	831	550
AmO_2^{+}	718	60

Chapter 4

Experimental Procedures

4.1 General

All reagents were reagent grade and used as received unless otherwise stated. The acids used were $HClO_4$ (GFS Chemicals or Mallinckrodt), HNO_3 (Baker), HCl (Baker), and HI (Aldrich or freshly distilled Baker with hydrazine(Aldrich) as preservative). The bases used were NH_3 (Mallinckrodt) and NaOH (GFS Chemicals). Other reagents were ethylenediaminetetraacetic acid (EDTA, Fisher), $Fe(NO_3)_3$ (Baker & Adamson), and $NaClO_4$ (GFS Chemicals). All dilutions or aqueous solutions were prepared using deionized and distilled water further purified by a Millipore cartridge system.

4.2 UO_2^{2+} Preparation

Natural uranium as reagent grade $U(NO_3)_6 \cdot 6H_2O$ (Spectrum) was dissolved in 7 M $HClO_4$ and fumed until almost solidified. The brown fumes from nitric acid were followed by white fumes from perchloric acid, because the boiling point of nitric acid is lower than perchloric acid. The solution was diluted with water and fumed twice again (no brown fumes were observed). The solution was then diluted using 0.01 M $HClO_4$. The isotopic abundances of natural uranium are presented in Table 4.1. Three UO_2^{2+} stock solutions were made; information on the uranium content of each is contained in Table 4.2.

Table 4.1: Isotopic abundances of natural uranium.

Isotope	Atom %	$t_{1/2}$, y	Decay mode	Activity %
^{238}U	99.2745	4.4683×10^9	α	48.17
^{235}U	0.720	7.03×10^8	α	2.25
^{234}U	0.0055	2.446×10^5	α	49.58

Table 4.2: Uranium stock solutions.

Stock Solution	Concentration, M	Total activity, μCi	Mass U, g
1	0.482 ± 0.014	0.394 ± 0.012	0.573 ± 0.005
2	0.539 ± 0.016	0.441 ± 0.013	0.642 ± 0.005
3	0.482 ± 0.005	1.971 ± 0.020	2.870 ± 0.005

4.3 NpO_2^+ Preparation

The following procedure was used for the dissolution and purification of $^{237}NpO_2$ (obtained from LLNL Nuclear Chemistry Division)[a]; it is a modification of previously published procedures [41, 42]. The elemental/isotopic analysis, determined using α spectroscopy, for the final ^{237}Np stock solution is given in Table 4.3. A total of 46.9 ± 1.2 mg of ^{237}Np was purified and a stock solution of 0.0990 ± 0.0025 M (total activity of 33.1 ± 0.8 μCi) was prepared. Both ^{238}Pu and ^{237}Np are produced by neutron irradiation of U followed by β^- decay. Complete separation of one element from the other is very difficult. The building in which the LIPAS measurements were performed would only allow a maximum of 1 μCi of activity from the ^{238}Pu contaminant and special permission had been obtained to allow the larger amount of ^{237}Np to be used.

The $^{237}NpO_2$ was dissolved in warm 8 M HNO_3. Ferrous sulfamate was used to insure that Np was in the +4 oxidation state and the excess $Fe(SO_3NH_2)_2$ was destroyed by heating the solution to 70° C. A Dowex A1, ×8 (100–140 mesh) anion exchange resin column was prepared and pre-treated with 8 M HNO_3 [41, pg. 89]. The Np^{4+} solution was sorbed on the column which was then washed with 8 M HNO_3. Uranium and Fe^{3+} are eluted from the column under these conditions. The column was washed with 10 M HCl, and the Pu was eluted by reduction to Pu^{3+} with a

[a]Performed by K. Moody and M. A. Stoyer.

solution one part 5 M HI and ten parts 10 M HCl [42]. The Np was then eluted using 0.5 M HCl. The resulting ^{237}Np solution was concentrated and then assayed via alpha spectroscopy.

The above mentioned assay showed that the ^{238}Pu activity in the ^{237}Np solution was greater than the imposed limit. The solution was dried and redissolved in 10 M HCl with a small amount of 4 M HNO_3. Another Dowex A1, $\times 8$ anion exchange resin column was prepared and pre-treated with 10 M HCl and the Np solution was passed through. The Pu was eluted with warm solution of one part 5 M HI and ten parts 10 M HCl [41, pp. 169-170]. Next, 8 M HNO_3 was used to remove any U that might be present. Finally, the Np was eluted using 0.5 M HCl. The solution was evaporated and dissolved in 10 M HCl twice and then assayed. Again the ^{238}Pu activity was too high; however, no other contaminant activities were found.

The Np solution was dried and dissolved in solution A (9 M HCl/0.05 M HNO_3). Another Dowex A1, $\times 8$ anion exchange resin column was prepared and pre-treated with solution A. The Np solution was sorbed on the column from solution A and washed with approximately 10 ml of solution A. The Np was eluted using 3 M HCl. The eluant was collected in nine fractions of about 35 ml each. The resulting fractions were assayed. A four-fraction combination ($\approx$ 150 ml total volume) contained enough Np with sufficient purity for our purposes. The volume was reduced to about 1 ml, $HClO_4$ added and fumed (until about 0.5 ml remained). The resulting solution was

Table 4.3: Elemental/isotopic abundances for ^{237}Np solution.

Isotope	Atom %	$t_{1/2}$, y	Decay mode	Activity %
^{237}Np	100	2.14×10^6	α	95.5
^{238}Pu	1.93×10^{-4}	87.71	α	4.5

diluted with 0.1 M $HClO_4$ to 2 ml total volume. This solution was then assayed for determination of the exact composition; the results are shown in Table 4.3.

4.4 PuO_2^+ and PuO_2^{2+} Preparation

The plutonium as ^{242}Pu was obtained from the Actinide Geochemistry Group at LBL. A anion exchange column was used for purification from any decay products or other actinide contaminants.

The Pu purification was accomplished using a modification of the procedure by D. C. Hoffman [42]. An AG-1, ×8 (Biorad) anion exchange column was prepared and pre-treated with 12 M HCl. The Pu contained in a small volume of a 6 M HCl solution was sorbed on the column while the +3 actinides run through and the column was washed with 10 M HCl. Plutonium was eluted using a solution of seven parts 12 M HCl and one part 4.4 M HI to reduce Pu^{4+} to Pu^{3+} which elutes. The Pu stock solution radioisotopic analysis, which was obtained using γ and α pulse-height analysis, is given in Table 4.4. The resulting Pu solution was then fumed with HNO_3 followed by $HClO_4$ to remove any iodine and convert it to a $HClO_4$ solution. The

final solution was about 0.1 M $HClO_4$. A total of 23.5 ± 0.5 mg ^{242}Pu was purified making a main stock solution of $1.94(4) \times 10^{-2}$ M Pu (total activity of 5.4 ± 0.1 mCi).

Two different Pu oxidation states were needed during these experiments. Plutonium in the +6 oxidation state was obtained by fuming with perchloric acid. The +5 oxidation state was obtained by reduction of PuO_2^{2+} electrochemically. The solution pH was adjusted to 3.0–3.3 and a 570 mV (vs. Ag/AgCl) potential was applied for at least 2 h [43]. The oxidation state purity was determined via absorption spectroscopy and compared with literature spectra [44]. These solutions were prepared as needed; generally the concentrations were approximately 10^{-3} M ($\approx$ 0.3 mg/ml of Pu and $\approx$ 30 μCi of activity).

Table 4.4: Elemental/isotopic abundances for ^{242}Pu solution.

Isotope	Atom %	$t_{1/2}$, y	Decay mode	Activity %
^{242}Pu	99.85	3.763×10^5	α	11.36
^{241}Pu	0.029	14.355	β^-, α	86.72
^{239}Pu	0.120	2.413×10^4	α	0.22
^{238}Pu	0.048	87.71	α	1.41
^{241}Am	0.01	432.0	α	0.30

4.5 Th^{4+} Preparation

Thorium nitrate (from J. E. Andrews, LLNL Nuclear Chemistry Division, HIPURE 99.99% ^{232}Th) was dissolved in 8 M nitric acid. An AG-1, $\times$8 (100–200 mesh) (Biorad)

anion exchange resin column was prepared and pre-treated with 8 M HNO_3. The Th^{4+} was sorbed from 8 M HNO_3 and the column was washed with 8 M HNO_3. The ^{232}Th daughters elute from the column under these conditions. The Th^{4+} was then eluted with dilute HCl (2 M or 0.1 M), fumed with perchloric acid until almost solidified, diluted with water and fumed twice again. The solid was then dissolved in 0.01 M $HClO_4$.

The resulting stock solutions were standardized using the following EDTA titration. A 0.2 ml aliquot of the Th^{4+} stock solution was diluted with about 100 ml water, pyrocatechol violet indicator was added (solution was blue); the solution was then acidified using 6 M HCl until the solution turned red. This solution was titrated with 0.0100 M EDTA until the solution turned yellow, indicating the end point. Information on each of the Th^{4+} stock solutions is contained in Table 4.5.

Table 4.5: Thorium stock solutions.

Stock solution	Concentration, M	Total activity, μCi	Mass, g
1	0.198 ± 0.002	0.051 ± 0.001	0.459 ± 0.005
2	0.544 ± 0.007	0.070 ± 0.001	0.631 ± 0.008

4.6 Fe^{3+} Preparation

Iron nitrate was dissolved in 7 M $HClO_4$. This solution was fumed until almost dry, water was added, and it was fumed three more times. The resulting solid was

dissolved in 0.01 M $HClO_4$.

The stock solution was standardized using a gravimetric procedure. An aliquot of the Fe solution was diluted to 5 ml with H_2O. This solution was made strongly alkaline using NH_4OH to precipitate Fe hydroxide. The precipitate was filtered on ashless filter paper, rinsed with 1.4 M NH_3 and then rinsed with methanol. The filter paper with the Fe precipitate was dried, charred, and then ignited in a porcelain crucible using a Bunsen burner prior to being placed in a desiccator for cooling. The concentration of the Fe stock solution was determined from the Fe_2O_3 weight and the dilution to be 1.35 ± 0.04 M Fe^{3+}.

4.7 Preparation of Experimental Solutions

The experimental solutions for LIPAS measurements were prepared from stock solutions of metal ions, acid, base, and $NaClO_4$ electrolyte. For specific information about the concentrations of the experimental solutions analyzed see the appropriate section in Chapter 5. The experimental solutions were prepared the day the LIPAS measurement was made and each one had a total volume of 1 ml. Solutions containing plutonium, neptunium, or uranium were kept above 0.001 M H^+ to prevent hydrolysis.

4.8 LIPAS Measurements

The entire experimental solution was placed in the PZT/cuvette assembly for measurement (See Chapter 3 for equipment details). The cuvette was rinsed with the reference solution (a $NaClO_4$ solution with the same ionic strength and approximately the same pH) prior to introducing the experimental solution. Before or after each experimental measurement, the reference solution was measured. Standards composed of a stable lanthanide ion were measured before the experiment to verify that the LIPAS equipment was operating properly. A stable lanthanide-ion standard was also measured between experimental solutions if verification of LIPAS operation was desired.

The preliminary set of experiments with a given complex system involved determining: (1) if the "ligand" had appreciable absorbance in the spectral region scanned; (2) if equilibrium was attained within a reasonable amount of time; (3) if there was evidence for complexation; and (4) if there were any other problems to solve. The "ligand" absorbance is important because the ligand is present at about two orders of magnitude greater concentrations than the AnO_2^+ and might interfere with our ability to detect the AnO_2^+ or any changes in its spectrum. Because actinides typically exchange the water molecules of their hydration sphere quickly, equilibrium is expected to occur almost instantaneously. Equilibrium was assumed when there was no change in the LIPAS spectra for three successive scans ($\approx$ 10 min/scan) taken im-

mediately after the solutions were prepared. If there was evidence for complexation, a more careful study might be warranted, depending on the result obtained. If no evidence for complexation was detected where expected, a careful examination of the procedure was performed to determine the course of action to follow. When problems were encountered during the preliminary experiment, it had to be determined if or how they could be overcome.

4.9 Data Treatment

Two methods were used to calculate the K_{eq} value for the cation-cation complexes, the computer code SQUAD (Section 4.9.1) and a manual calculation (Section 4.9.2). Both methods use the same information and the same data treatment for the raw data. Initial AnO_2^+ and ligand concentrations are known from the dilution of stock solutions. All absorption spectra are an average of up to three background-subtracted spectra obtained from the data acquisition program LASER[b]. The absorbance spectra used for Beer's Law plots are for standard solutions containing only the AnO_2^+ species at different concentrations. Using the relationship in Eq. 3.8, the $\mathcal{K}^\lambda$ is calculated for each standard solution at all wavelengths; these results are then averaged to obtain the values for $\mathcal{K}^\lambda$ as a function of λ. The $\mathcal{K}^\lambda$ values can be used to generate a calculated AnO_2^+ spectrum of any concentration. Where necessary, the experimental solutions

[b]See page 38 for more information on the data acquisition program.

are normalized at a specific wavelength to a solution with similar AnO_2^+ concentration as noted in the discussion for each specific experiment. Normalization was performed when a baseline shift had occurred in the spectrum. The isosbestic point[c] is the best wavelength for normalization because all spectra with the same initial concentration of AnO_2^+ will show the same absorbance; however, the isosbestic point is not always obvious. A wavelength away from the peak will be used if the isosbestic point is not apparent; a reasonable normalization wavelength is indicated by the presence of an isosbestic point after normalization. Occasionally normalization is performed to demonstrate that the spectra have the same shape regardless of baseline shifts.

4.9.1 SQUAD

SQUAD was written by D. J. Leggett (see [45] for a complete discussion). The version used in this thesis was modified by R. A. Torres (LLNL, Chemistry and Materials Science Division). The modifications were fairly minor (no changes in the sections of the code which perform the actual calculations) and involved: (1) formatting of the screen output, file output, and file input; (2) changing the allowable number range (computer limit); (3) changing the number of data points per spectrum; (4) allowing user generated output file names; (5) disabling the printer plots of the data; (6) enabling grid search option instead of card punching option; and (7) setting lower limits

[c]Given that X is converted to Y during the course of a reaction and the spectra of pure X and pure Y cross at some wavelength, $\lambda_{i.p.}$, $\varepsilon_X^{\lambda_{i.p.}} = \varepsilon_Y^{\lambda_{i.p.}}$. If [X] + [Y] is constant, all spectra containing X, Y, or a mixture of X and Y will intersect at $\lambda_{i.p.}$.

on the amount that the $\log(K_{eq})$ can be changed during each iteration.

SQUAD, using the initial metal and ligand concentrations, the experimental absorption spectra (normalized if necessary), known absorption spectra ($\mathcal{K}^{\lambda}$ values), and a reaction model, calculates the desired equilibrium constants, absorption spectra, free metal and ligand concentrations, and complex concentrations using either a multiple regression algorithm or a non-negative least squares algorithm (user's choice). This program has the capability of determining equilibria for up to six complex species with the general form $M_m M'_l H_j L_n L'_Q$ where m, l, n, $q \geq 0$ and j is positive (protons), negative (hydroxide ions), or zero. For each absorbance,

$$A_{i,k} = \sum_{1}^{J} [\text{species}]_{i,j} \times \varepsilon_{j,k},$$

where $[\text{species}]_{i,j}$ is the concentration of the jth species in the ith spectrum and $\varepsilon_{j,k}$ is the molar absorptivity of the jth species at the kth wavelength, SQUAD minimizes

$$U = \sum_{1}^{K} \sum_{1}^{I} (A_{i,k}^{\text{obs}} - A_{i,k}^{\text{calc}})^2,$$

which is the sum of the difference between the observed and calculated absorbance values squared (residuals squared).

4.9.2 Manual K_{eq} Calculation

This method is used as an initial determination of the approximate K_{eq} for a complex. In some cases SQUAD did not converge and this method provided the only

K_{eq} measurement. Where SQUAD did converge, this method provides an additional measurement of K_{eq}.

Provided the species in question are truly 1:1 complexes, the reaction is

$$AnO_2^+ + M^{n+} \rightleftharpoons AnO_2^+ \cdot M^{n+},$$

where AnO_2^+ is UO_2^+, NpO_2^+, PuO_2^+, or AmO_2^+, and M^{n+} (the ligand) is one of many cations including the actinyl ions. The equilibrium constant for such a reaction is given by

$$K_{eq} = \frac{[AnO_2^+ \cdot M^{n+}]}{[AnO_2^+] \cdot [M^{n+}]},$$

with units of M^{-1}. Assuming that the initial AnO_2^+ concentration is negligibly small compared to the initial ligand cation concentration, the fraction of the AnO_2^+ complexed is given by:

$$\frac{[AnO_2^+ \cdot M^{n+}]}{[AnO_2^+]_{initial}} = \frac{K_{eq}[M^{n+}]}{(1 + K_{eq}[M^{n+}])}, \tag{4.1}$$

which indicates that the ligand concentration is very important for the formation of cation-cation complexes under these conditions. Rearranging Eq. 4.1 gives

$$K_{eq} = \frac{R}{(1 - R)[M^{n+}]}, \tag{4.2}$$

where

$$R = \frac{[AnO_2^+ \cdot M^{n+}]}{[AnO_2^+]_{initial}},$$

a dimensionless ratio. Assuming Eq. 3.8 is true, R can also be calculated using $S_i^{\lambda max}$, the photoacoustic signal from the initial AnO_2^+ concentration, and $S_e^{\lambda max}$, the

photoacoustic signal for the uncomplexed AnO_2^+ at equilibrium, using

$$R = \frac{S_i^{\lambda max} - S_e^{\lambda max}}{S_i^{\lambda max}},$$

where λ_{max} is the wavelength for the maximum absorbance for the AnO_2^+ species. The above is only true if the cation-cation complex has no absorbance at the λ_{max} of the AnO_2^+ species; therefore, it is only an approximation. If the cation-cation complex has some absorbance at λ_{max} of the AnO_2^+ species, the K_{eq} calculated using this manual method will tend to be low because some of the absorbance assigned to the uncomplexed AnO_2^+ is actually due to the complex. The uncertainty in the K_{eq} calculated in this way is expected to be large not only because of the possibility of complex absorbance at the AnO_2^+ peak, but also because in some instances the absorbances of the initial and equilibrium peaks are almost the same.

Chapter 5

Results and Discussion

The results of the seven studies conducted will be discussed in this chapter. Most of the studies were conducted in a 6 M ionic strength aqueous solutions with $NaClO_4$ as the background electrolyte; deviations from this will be noted. Unless otherwise stated, for these systems the M^{n+} species did not have appreciable absorbance in the region of interest for complex formation, kinetics were fast, there was evidence for complexation, and no pertinent problems were discovered. All experiments were conducted using the same LIPAS system installed in an inert atmosphere glove box.

5.1 $NpO_2^+ \cdot UO_2^{2+}$ Complex

Four previous publications reported K_{eq} values for the $NpO_2^+ \cdot UO_2^{2+}$ complex. The ionic strengths used were 3.0, 6.0, 6.26, and 7 M with K_{eq} values of 0.69 ± 0.01, 2.25 ± 0.03, 2.5 ± 0.5, and 3.7 ± 0.1 M^{-1}, respectively (see Table 2.1).

In this research, the $NpO_2^+ \cdot UO_2^{2+}$ complex was studied at two different ionic

strengths. For the initial experiments, a low ionic strength was used, to determine if cation-cation complexes form under these conditions also. Even though formation of cation-cation complexes in lower ionic strengths solutions has not been reported, a sensitive technique like LIPAS might be able to detect complex formation even in low ionic strength solutions. Sensitivity to changes in the NpO_2^+ peak (616.0 nm), either amplitude or peak shape, of a couple percent would be necessary and LIPAS can provide this sensitivity.

5.1.1 Low Ionic Strength

The solutions used for this experiment are shown in Table 5.1. Shown in Fig. 5.1 are portions of two spectra, pure NpO_2^+ (solid line, calculated using the $\mathcal{K}^\lambda$) and a mixture of NpO_2^+ and UO_2^{2+}(dashed line, solution A-3 in Table 5.1). These spectra were normalized at 623.0 nm. For the spectrum for solution A-3, a small decrease in the height and increase in the width on the lower wavelength side of the peak is observed. This change could be due to cation-cation complex formation because the spectral change is similar to the change observed in the higher μ solutions described in Section 5.1.2. It should be noted that the μ of the two spectra are not exactly the same because the large concentration of UO_2^{2+} used increased the ionic strength. The K_{eq} for the $NpO_2^+ \cdot UO_2^{2+}$ complex at $\mu < 1$ M is small. Assuming that the spectral changes in solutions A-1, A-2, and A-3 described in Table 5.1 are due to cation-cation

complexation, an approximate K_{eq} can be calculated from the $S^{616.0}$ obtained for each solution at the NpO_2^+ peak and the $S^{616.0}$ from pure NpO_2^+ solutions from Eq. 4.2. The average K_{eq} calculated by the manual method for all three solutions is approximately 0.3 M^{-1}. The wavelength with the maximum absorbance, λ_{max}, for the complex is in the range 613–615 nm; the amount that the λ_{max} is shifted in going from the uncomplexed species to the complexed species, $\Delta\lambda^a$, is 1–3 nm. This calculated K_{eq} for $NpO_2^+ \cdot UO_2^{2+}$ at < 1 M is reasonable because it would be expected to be smaller than the previously reported K_{eq} of 0.69 ± 0.01 M^{-1} determined at $\mu = 3$ M [5] for the $NpO_2^+ \cdot UO_2^{2+}$ cation-cation complex (see Table 2.4).

Table 5.1: Experimental solutions for $NpO_2^+ \cdot UO_2^{2+}$ complex at $\mu < 1$ M.

Solution	$[NpO_2^+]_i$, mM	$[UO_2^{2+}]_i$, M	K_{eq}†, M^{-1}
Standards			
Np-1	0.248 ± 0.012		
Np-2	0.099 ± 0.005		
U-1		0.0867 ± 0.0043	
Mixtures			
A-1	0.248 ± 0.012	0.0867 ± 0.0043	≈ 0.4
A-2	0.248 ± 0.012	0.260 ± 0.013	≈ 0.2
A-3	0.495 ± 0.025	0.260 ± 0.013	≈ 0.2
			Ave. ≈ 0.3

† — calculated using manual method of Eq. 4.2.

[a] $\Delta\lambda = | \lambda_{max,\text{complex}} - \lambda_{max,AnO_2^+} |$.

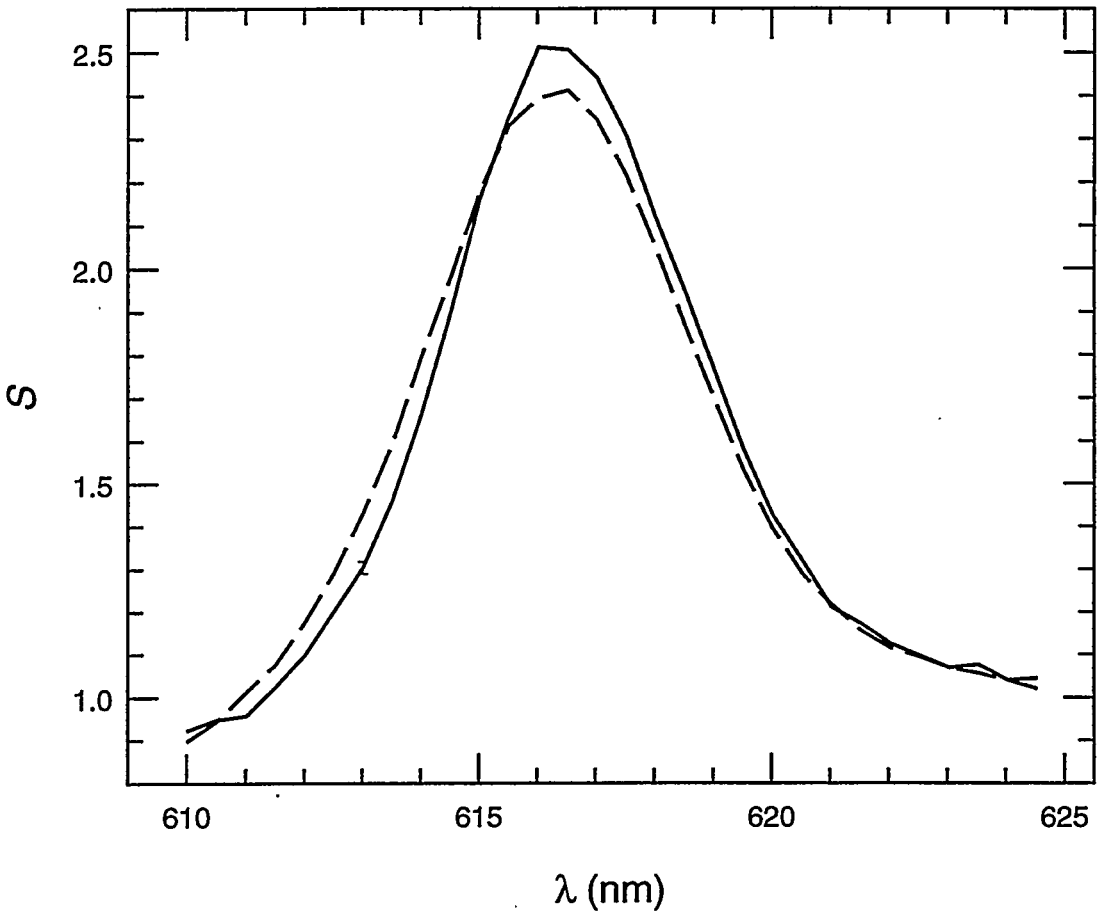

Figure 5.1: Spectra for the $NpO_2^+ \cdot UO_2^{2+}$ complex experiment at $\mu < 1$ M. The spectra shown are for a calculated NpO_2^+ concentration of 0.495 mM (solid line) and solution A-3 (dashed line). See Table 5.1 for the composition of solution A-3. The spectra are normalized at 623.0 nm. The error bar at 613.0 nm on the solid line is typical of the errors for these spectra. Note the ordinate scale does not begin at 0.

5.1.2 6 M Ionic Strength

The first $NpO_2^+ \cdot UO_2^{2+}$ experiment at $\mu = 6$ M indicated a shoulder on the lower wavelength side of the NpO_2^+ 617 nm peak; further experiments were conducted to investigate this effect. Enhancement was attempted by increasing the ratio of UO_2^{2+} to NpO_2^+ by using lower NpO_2^+ concentration while maintaining the UO_2^{2+} concentrations at the same levels as for the preliminary experiment. This proved to be unfruitful. However, increasing the amount of UO_2^{2+} present produced the results presented below. This is consistent with the formation of a cation-cation complex where the K_{eq} is defined by Eq. 2.1 and Eq. 4.1 is also valid.

For the experiment outlined in Table 5.2, the experimental solution spectra were normalized at 607.0 nm. Using SQUAD, a K_{eq} of 2.4 ± 0.2 M^{-1} was calculated with the $NpO_2^+ \cdot UO_2^{2+}$ complex λ_{max} at 613.0 nm ($\Delta\lambda = 4.0$ nm). This K_{eq} result agrees with the literature value of 2.25 ± 0.03 M^{-1} at $\mu = 6$ M (see Table 2.4). The spectra used for the SQUAD calculation are shown in Fig. 5.2.

The K_{eq} was also calculated using Eq. 4.2 and the results are shown in Table 5.2. They are clearly consistent with the K_{eq} from the SQUAD calculation and those reported in the literature.

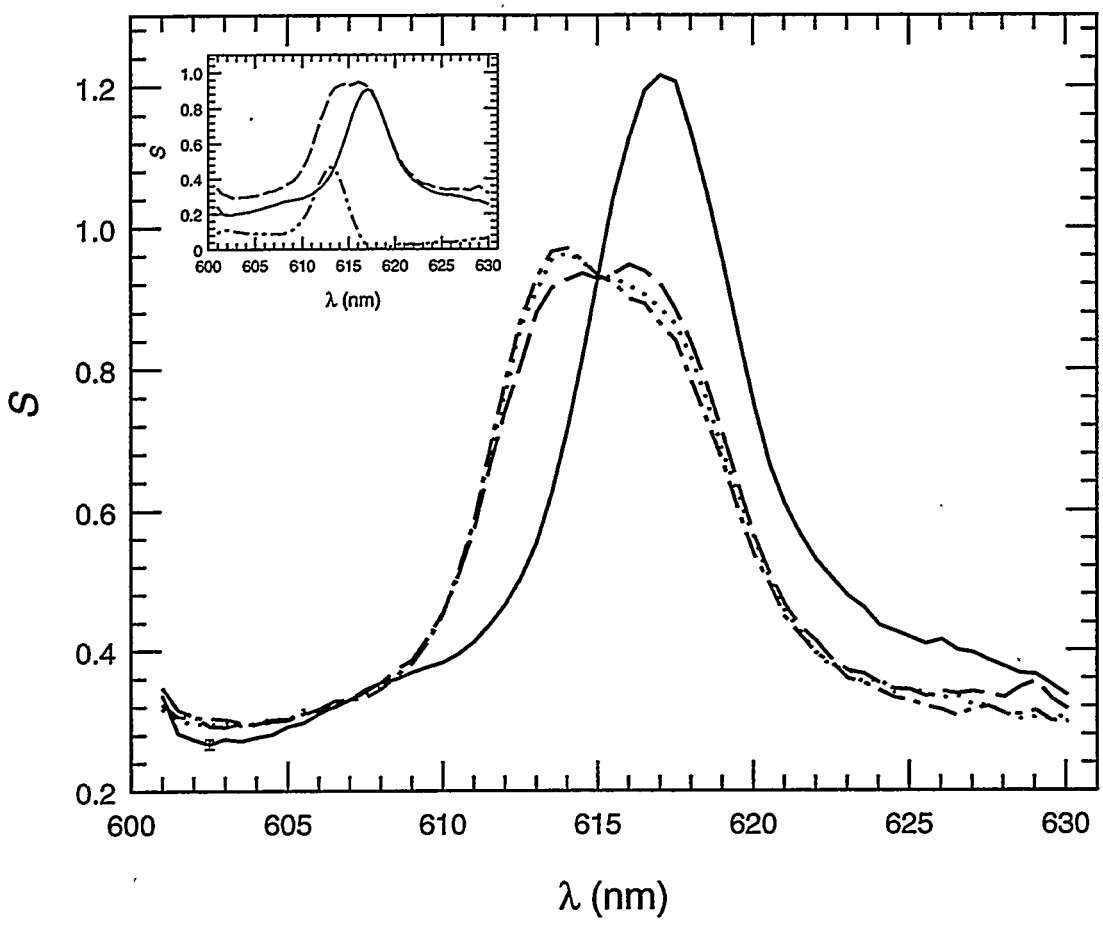

Figure 5.2: Spectra for the $NpO_2^+ \cdot UO_2^{2+}$ complex experiment at $\mu = 6$ M. The spectra shown are for a calculated NpO_2^+ concentration of 0.248 mM (solid line), solution B-1 (dot-dashed line), solution B-2 (dotted line), and solution B-3 (dashed line). See Table 5.2 for the compositions of B-1, B-2, and B-3. The spectra were normalized at 607.0 nm. The error bar at 602.5 nm on the solid line is typical for these spectra. Not the ordinate scale does not begin at 0. Shown in the inset is a deconvoluted spectrum using the results obtained from SQUAD. The spectra shown are solution B-3 (dashed line), the contribution from the uncomplexed NpO_2^+ (solid line), and the contribution from the $NpO_2^+ \cdot UO_2^{2+}$ complex (dot-dot-dashed line).

Table 5.2: Experimental solutions for $NpO_2^+ \cdot UO_2^{2+}$ complex at $\mu = 6$ M.

Solution	$[NpO_2^+]_i$, mM	$[UO_2^{2+}]_i$, M	K_{eq}†, M^{-1}
Standards			
Np-3	0.297 ± 0.015		
Np-4	0.198 ± 0.010		
Np-5	0.149 ± 0.007		
U-2		0.149 ± 0.007	
Mixtures			
B-1	0.248 ± 0.012	0.178 ± 0.009	≈ 2.3
B-2	0.248 ± 0.012	0.162 ± 0.008	≈ 2.3
B-3	0.248 ± 0.012	0.146 ± 0.007	≈ 2.2

† — calculated using manual method of Eq. 4.2.

5.2 $NpO_2^+ \cdot Th^{4+}$ Complex

The $NpO_2^+ \cdot Th^{4+}$ cation-cation complex had been reported previously in two different publications [12, 23]; however, neither gave a measured K_{eq}. For the experiment outlined in Table 5.3, a K_{eq} of 1.8 ± 0.9 M^{-1} was calculated using SQUAD. The $NpO_2^+ \cdot Th^{4+}$ complex was calculated to have a λ_{max} of 614.0 nm ($\Delta\lambda = 3$ nm). These data did not require any normalization and the spectra used for the SQUAD calculation are shown in Fig. 5.3. Calculations of K_{eq} using Eq. 4.2, the manual method, are shown in Table 5.3 and gave approximately 0.9 M^{-1}, within the error limits of the SQUAD calculation.

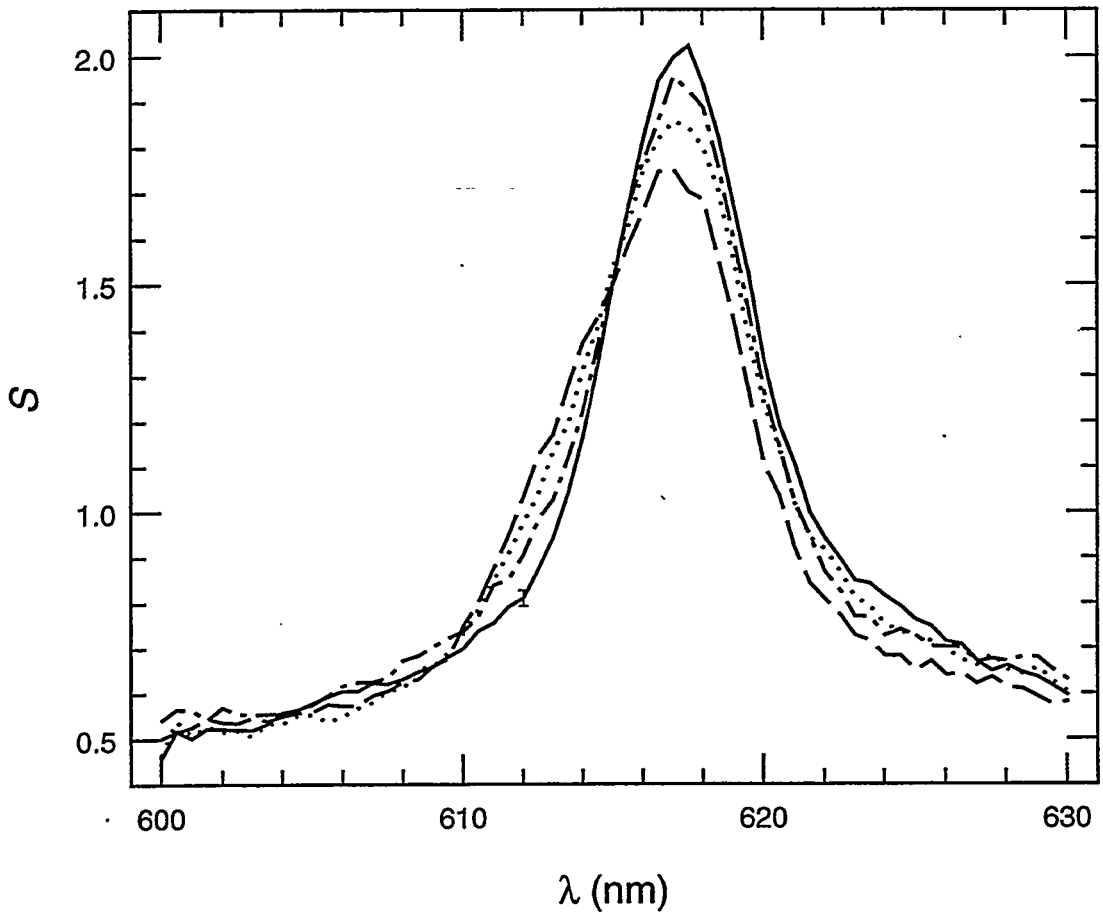

Figure 5.3: Spectra for the $NpO_2^+ \cdot Th^{4+}$ complex experiment at $\mu = 6$ M. The spectra shown are for a calculated NpO_2^+ concentration of 0.297 mM (solid line), solution C-1 (dashed line), solution C-2 (dotted line), and solution C-3 (dot-dashed line). See Table 5.3 for the compositions of C-1, C-2, and C-3. The spectra did not require any normalization. The error bar at 612.0 nm on the solid line is typical for these spectra. Note the ordinate scale does not begin with 0.

Table 5.3: Experimental solutions for $NpO_2^+ \cdot Th^{4+}$ complex at $\mu = 6$ M.

Solutions	$[NpO_2^+]_i$, mM	$[Th^{4+}]_i$, M	K_{eq}†, M^{-1}
Standards			
Np-6	0.396 ± 0.020		
Np-7	0.297 ± 0.015		
Np-8	0.198 ± 0.010		
Th-1		0.211 ± 0.011	
Th-2		0.0544 ± 0.0027	
Mixtures			
C-1	0.297 ± 0.015	0.218 ± 0.011	≈ 0.9
C-2	0.297 ± 0.015	0.1088 ± 0.0054	≈ 0.9
C-3	0.297 ± 0.015	0.0544 ± 0.0027	≈ 0.9

† — calculated using manual method of Eq. 4.2.

5.3 $PuO_2^+ \cdot UO_2^{2+}$ Complex

The $PuO_2^+ \cdot UO_2^{2+}$ complex had not been reported previously. These experiments were more difficult to perform than the ones described earlier. Because PuO_2^+ disproportionates into PuO_2^{2+} and Pu^{4+}(rate is dependant upon the fourth power of the hydrogen ion concentration so it is much faster at low pH), solutions containing PuO_2^+ were kept at a pH between 2 and 4 to extend the chemical lifetime of the PuO_2^+. These experiments also had to be conducted under an inert atmosphere (Ar) to prevent O_2 from reacting with the PuO_2^+. The solutions containing UO_2^{2+} and PuO_2^+ also had to be kept at a pH between 2 and 3 to prevent the UO_2^{2+} from undergoing hydrolysis. Preliminary experiments included taking LIPAS data in the region where the PuO_2^{2+} species absorbs to determine if appreciable disproportionation was occurring. These

results indicated that even a day after preparation of the solutions very little disproportionation had occurred. For the experimental solutions detailed in Table 5.4, the SQUAD calculations yielded a K_{eq} of 2.2 ± 1.5 M^{-1}. The λ_{max} for the $PuO_2^+ \cdot UO_2^{2+}$ complex determined by SQUAD was 564.5 nm ($\Delta\lambda = 5.5$ nm). Each experimental solution was normalized at 567.5 nm, the isosbestic point determined from solutions D-2 and D-3 (see Table 5.4). The experimental spectra that SQUAD used for its calculations along with a 0.0924 mM PuO_2^+ spectrum calculated from the $\mathcal{K}^\lambda$ are shown in Fig. 5.4. The average of the K_{eq}'s calculated using Eq. 4.2 is approximately 0.8 M^{-1}, again low as expected but still within the errors of the SQUAD calculation.

Table 5.4: Experimental solutions for $PuO_2^+ \cdot UO_2^{2+}$ complex at $\mu = 6$ M.

Solution	$[PuO_2^+]_i$, mM	$[UO_2^{2+}]_i$, M	K_{eq}†, M^{-1}
Standards			
Pu-1	0.0231 ± 0.0012		
Pu-2	0.0462 ± 0.0023		
Pu-3	0.0693 ± 0.0035		
Pu-4	0.0924 ± 0.0046		
Pu-5	0.139 ± 0.007		
U-3		0.0964 ± 0.0048	
Mixtures			
D-1	0.0553 ± 0.0028	0.144 ± 0.007	≈ 0.7
D-2	0.0924 ± 0.0046	0.0964 ± 0.0048	≈ 0.9
D-3	0.0924 ± 0.0046	0.0482 ± 0.0024	≈ 0.8

† — calculated using manual method of Eq. 4.2.

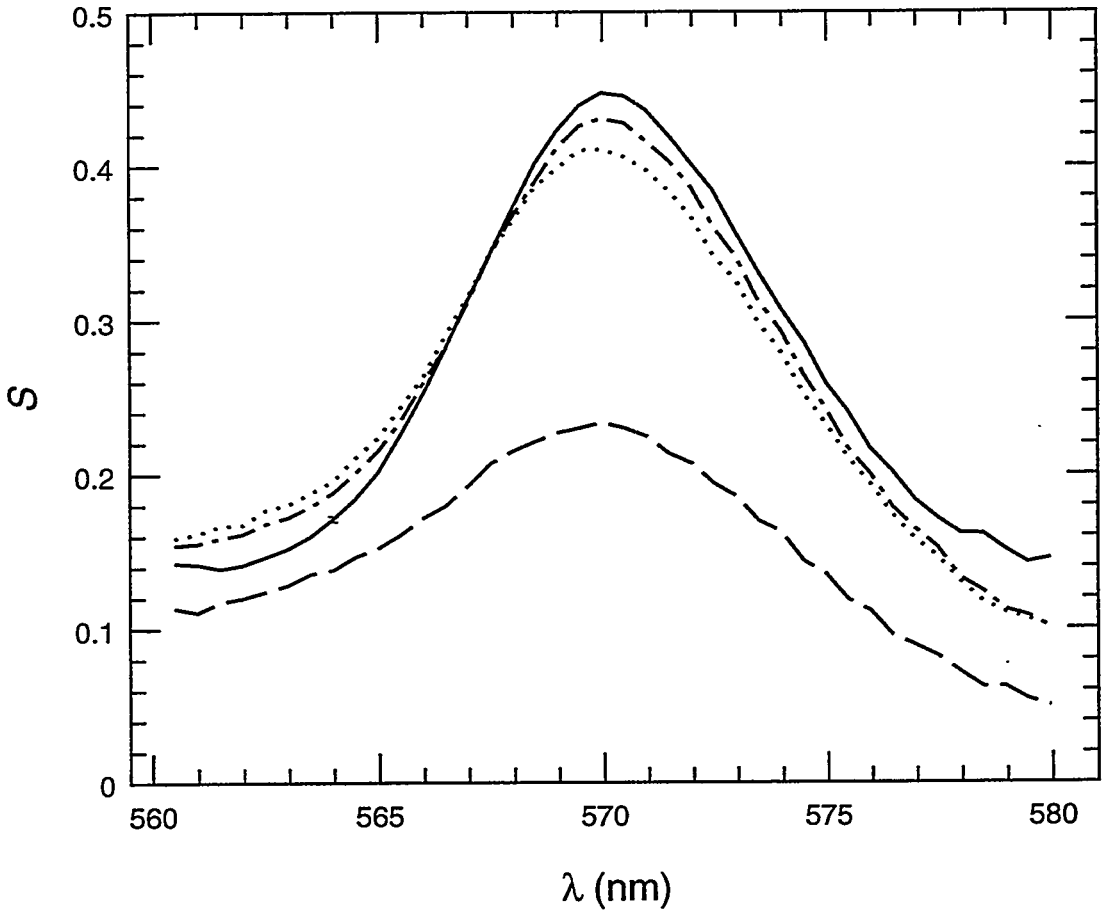

Figure 5.4: Spectra for the $PuO_2^+ \cdot UO_2^{2+}$ complex experiment at $\mu = 6$ M. The spectra shown are for a calculated PuO_2^+ concentration of 0.0924 mM (solid line), solution D-1 (dashed line), solution D-2 (dotted line), and solution D-3 (dot-dashed line). See Table 5.4 for the composition of solutions D-1, D-2, and D-3. Spectra are normalized at 567.5 nm, the isosbestic point. The error bar at 567.5 nm on the solid line is typical of the errors for these spectra.

5.4 $PuO_2^+ \cdot Th^{4+}$ Complex

The $PuO_2^+ \cdot Th^{4+}$ complex had not been previously reported. These experiments have many of the same problems of the $PuO_2^+ \cdot UO_2^{2+}$ complex experiments discussed in Section 5.3, with one added complication; Th^{4+} hydrolyzes at even lower pH, therefore solutions containing Th^{4+} needed a pH very close to 2. These experiments also included collection of LIPAS data in the region where PuO_2^{2+} absorbs to insure that the PuO_2^+ was not disproportionating extensively. For the experiment outlined in Table 5.5, SQUAD was not able to converge on a value for K_{eq}. Part of the reason is because these data do not have a clear isosbestic point (neither did the preliminary experiment) and the numerous attempts to normalize the data did not make it any clearer. As can be seen in Fig. 5.5, there does appear to be absorbance possibly due to a complex around 562 nm. However, one can use Eq. 4.2 to manually calculate an approximate K_{eq} value. The average K_{eq} is approximately 0.8 M^{-1}. It should be noted that the calculated K_{eq} values are not completely consistent among themselves, two distinct groups appear; this could also have contributed to the inability of SQUAD to converge. Although no PuO_2^+ disproportionation was detected, disproportionation of PuO_2^+ could affect the spectra and generate the problems encountered.

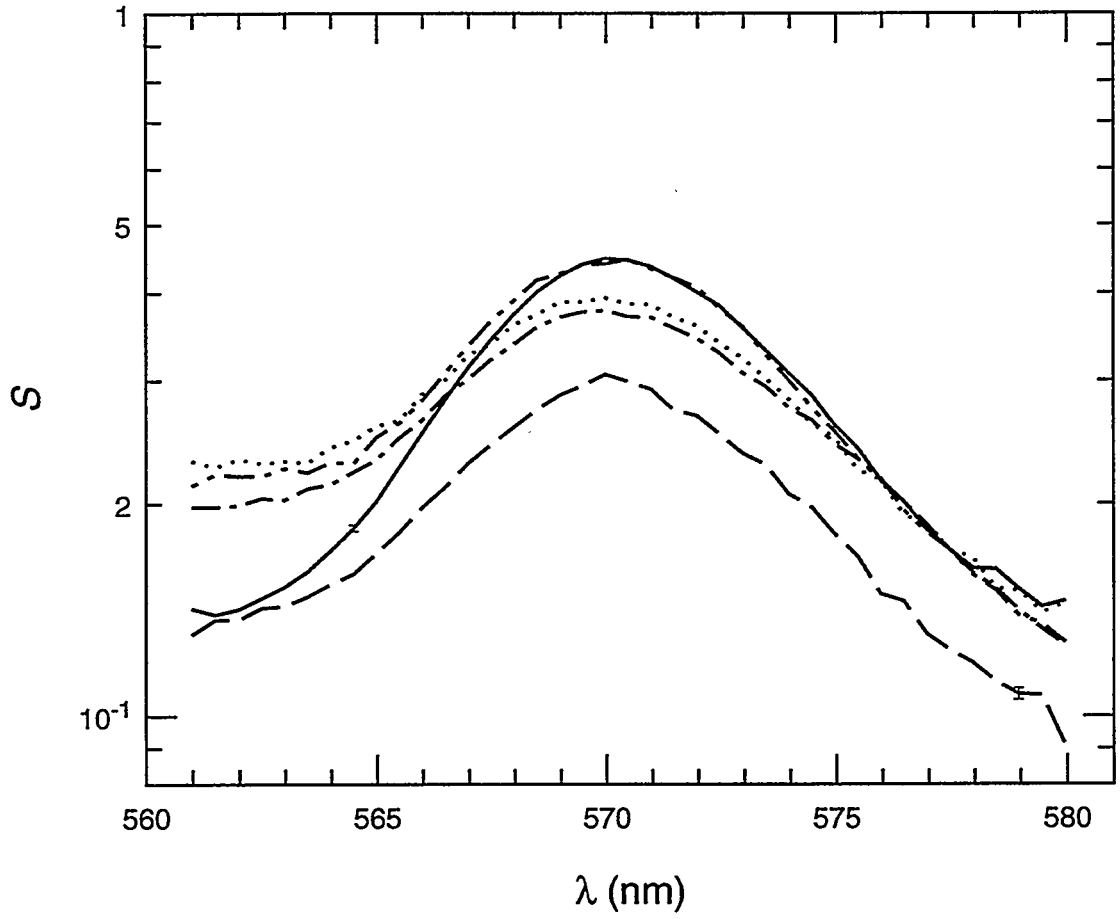

Figure 5.5: Spectra for the PuO_2^+·Th^{4+} complex experiment at $\mu = 6$ M. The spectra shown are for a calculated PuO_2^+ concentration of 0.0924 mM (solid line), solution E-1 (dashed line), solution E-2 (dot-dashed line), solution E-3 (dotted line), and solution E-4 (dot-dot-dashed line). See Table 5.5 for the composition of solutions E-1, E-2, E-3, and E-4. The error bars at 564.5 nm on the solid line and at 579.0nm on the dashed line are typical of the error for these spectra. Note that the ordinate is a log scale.

Table 5.5: Experimental solutions for $PuO_2^+ \cdot Th^{4+}$ complex at $\mu = 6$ M.

Solution	$[PuO_2^+]_i$, mM	$[Th^{4+}]_i$, M	K_{eq}†, M^{-1}
Standards			
Pu-6	0.0231 ± 0.0012		
Pu-7	0.0462 ± 0.0023		
Pu-8	0.0693 ± 0.0035		
Pu-9	0.0924 ± 0.0046		
Pu-10	0.139 ± 0.007		
Th-3		0.0544 ± 0.0027	
Th-4		0.0272 ± 0.0014	
Mixtures			
E-1	0.0668 ± 0.0033	0.197 ± 0.010	≈ 0.3
E-2	0.0924 ± 0.0046	0.163 ± 0.008	≈ 1.1
E-3	0.0924 ± 0.0046	0.109 ± 0.005	≈ 1.3
E-4	0.0924 ± 0.0046	0.0544 ± 0.003	≈ 0.3
			Ave. ≈ 0.8

† — calculated using manual method of Eq. 4.2.

5.5 $PuO_2^+ \cdot NpO_2^+$ Complex

The $PuO_2^+ \cdot NpO_2^+$ complex has never been reported. Over the wavelength range from 561 to 580 nm, LIPAS data could not be obtained even with a NpO_2^+ concentration of 0.0287 ± 0.0014 M. The PZT signal was so large that the preamplifier could not process the signal. Using Eq. 4.1, and assuming a K_{eq} of 1, about 0.028 of the PuO_2^+ is complexed when the NpO_2^+ concentration is 0.0287 M, which would be difficult to observe even under the most favorable of circumstances. Searching for a $PuO_2^+ \cdot NpO_2^+$ complex is especially difficult because at higher concentrations of NpO_2^+ the $NpO_2^+ \cdot NpO_2^+$ complex will also be present.

This experiment is actually a case where the increased sensitivity of LIPAS is a disadvantage. It might be possible to modify the electronics of the LIPAS system to allow this experiment to be conducted or it might be possible to use CAS for this experiment. If CAS was used more Pu would be necessary which might introduce other problems.

5.6 $PuO_2^+ \cdot Fe^{3+}$ Complex

A $PuO_2^+ \cdot Fe^{3+}$ intermediate had been indicated during a kinetic study [27]. Even though a H^+ concentration of 0.1 M was needed to prevent Fe^{3+} from hydrolysing and PuO_2^+ should disproportionate at such an H^+ concentration, the experiment was attempted. The experimental solutions are outlined in Table 5.6. Regions were scanned to investigate the PuO_2^+ species and the PuO_2^{2+} species. A Beer's law plot for the PuO_2^+ standard solutions was linear and spectra of the PuO_2^{2+} region indicated the presence of PuO_2^{2+} in all solutions. Three unnormalized spectra are shown in Fig. 5.6. The iron absorbance is very large and would mask the presence of any PuO_2^+ peak. From the spectra of the PuO_2^+ standards in both regions scanned, it is apparent that the H^+ concentration required for Fe^{3+} stabilization prevents PuO_2^+ from surviving for any appreciable length of time. A $PuO_2^+ \cdot Fe^{3+}$ complex will have to be investigated using a different method. It should be noted that the dye used, R590, was reaching the end of its useful lifetime; this is indicated by the large fluctuations and errors in

the region above approximately 574 nm.

Table 5.6: Experimental solutions for PuO_2^+·Fe^{3+} at $\mu = 6$ M.

Solution	$[PuO_2^+]_i$, mM	$[Fe^{3+}]_i$, M
Standards		
Pu-11	0.0439 ± 0.0022	
Pu-12	0.0585 ± 0.0029	
Pu-13	0.0293 ± 0.0015	
Pu-14	0.0351 ± 0.0018	
Fe-1		0.0338 ± 0.0017
Fe-2		0.0270 ± 0.0014
Fe-3		0.0203 ± 0.0010
Fe-4		0.0135 ± 0.0007
Mixtures		
G-1	0.0439 ± 0.0022	0.0338 ± 0.0017
G-2	0.0439 ± 0.0022	0.0270 ± 0.0014
G-3	0.0439 ± 0.0022	0.0203 ± 0.0010
G-4	0.0439 ± 0.0022	0.0135 ± 0.0007

5.7 UO_2^{2+} with Th^{4+}

Because UO_2^{2+} and Th^{4+} are not expected to form a cation-cation complex with each other, a null experiment was attempted. The region 415–445 nm containing the UO_2^{2+} peak at 427 nm was scanned. No evidence was found for complexation. A summary of the experiment is given in Table 5.7. The spectra normalized at 431.0 nm for all solutions containing Th^{4+} and UO_2^{2+} along with the spectrum for the same concentration of UO_2^{2+} are shown in Fig. 5.7; normalization was performed to allow easy comparison of the spectra shapes. As clearly indicated by the spectra

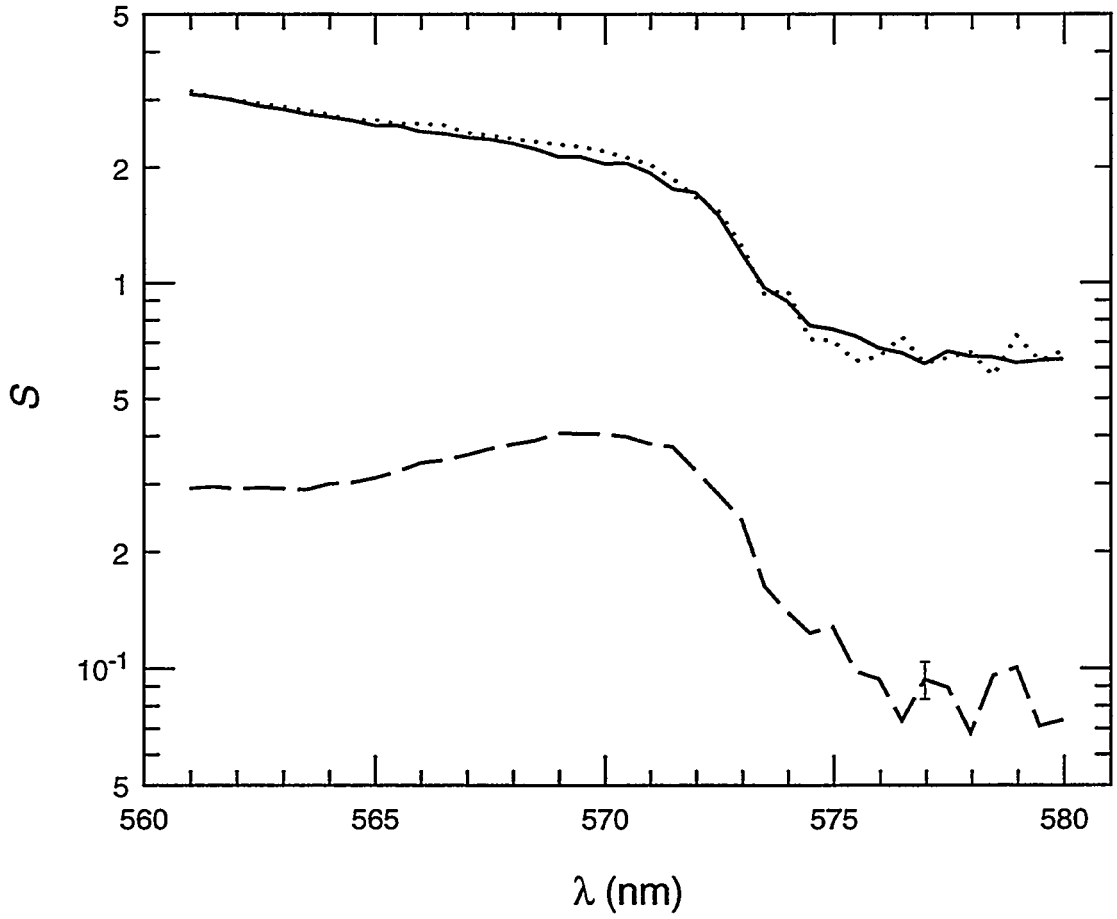

Figure 5.6: Spectra for the $PuO_2^+ \cdot Fe^{3+}$ experiment at $\mu = 6$ M. The spectra shown are for solution Pu-11 (dashed line), solution Fe-2 (solid line), and solution G-2 (dotted line). See Table 5.6 for the composition of the solutions. Spectra have not been normalized. The error bar at 577.0 nm on the dashed line is typical of the error for these spectra above about 574 nm; the error bars below about 574 nm are about the width of the line.

in Fig. 5.7, there is no indication of any species other than UO_2^{2+}. Notice again the larger fluctuations and error bar in the region below approximately 420 nm; this is close to the edge of the S420 lasing region and S420 has a relatively short lifetime so it was also nearing the end of its usefulness.

Table 5.7: Experimental solutions for UO_2^{2+} with Th^{4+} at $\mu = 6$ M.

Solution	$[UO_2^{2+}]_i$, mM	$[Th^{4+}]_i$, M
Standards		
U-4	1.93 ± 0.10	
U-5	1.45 ± 0.07	
U-6	0.96 ± 0.05	
U-7	0.48 ± 0.02	
Th-5		0.0673 ± 0.0034
Mixtures		
H-1	1.45 ± 0.07	0.0673 ± 0.0034
H-2	1.45 ± 0.07	0.0594 ± 0.0030
H-3	1.45 ± 0.07	0.0396 ± 0.0020
H-4	1.45 ± 0.07	0.0198 ± 0.0010

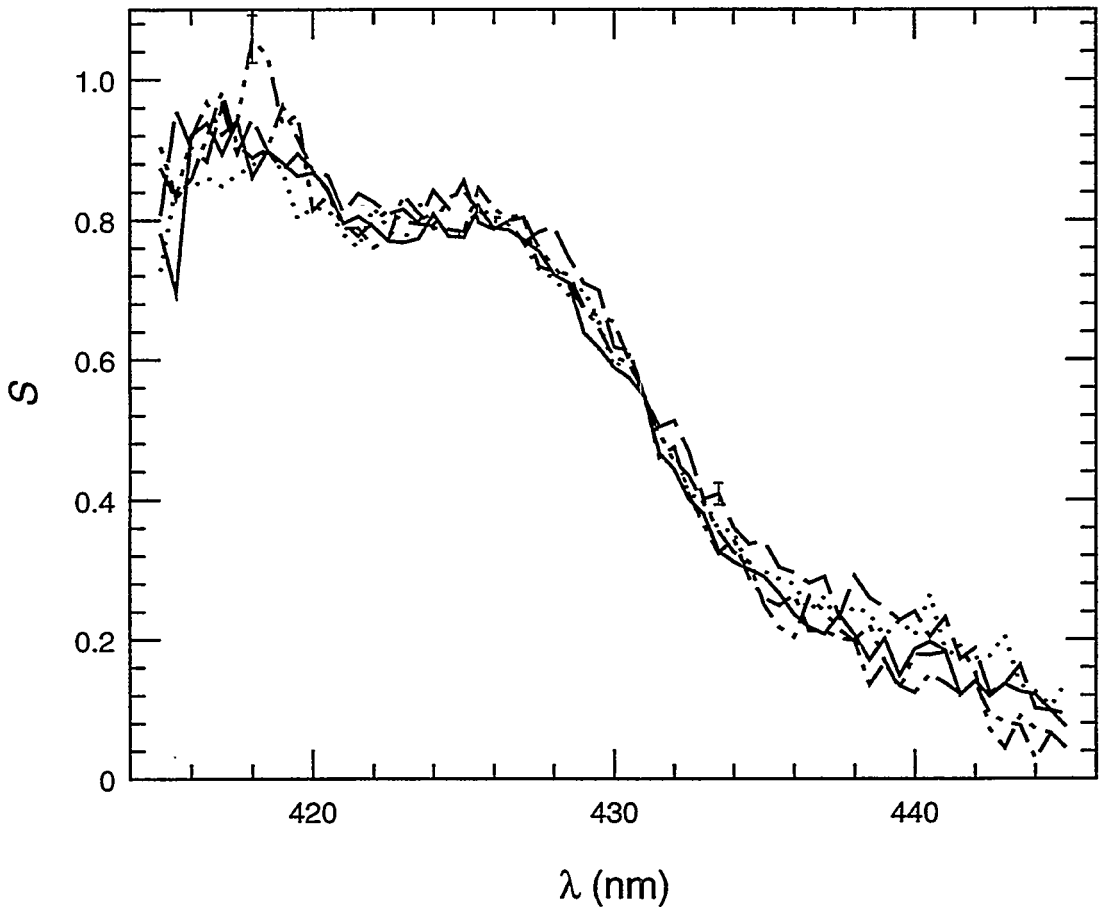

Figure 5.7: Spectra for the UO_2^{2+} with Th^{4+} experiment at $\mu = 6$ M. The spectra shown are for solution U-5 (solid line), solution H-1 (dashed line), solution H-2 (dotted line), solution H-3 (dot-dashed line), and solution H-4 (dot-dot-dashed line). See Table 5.7 for the composition of the solutions. Spectra are normalized at 431.0 nm. The error bars at 433.5 nm on the dashed line and at 418.0 nm on the dot-dot-dashed line are typical for these spectra in those regions.

Chapter 6

Conclusions

6.1 LIPAS Results

Absorption spectroscopy is a widely used technique to determine equilibrium constants, K_{eq}. LIPAS is a relatively new absorption spectroscopy technique that has not been used previously to determine the K_{eq} of a cation-cation complex. The known K_{eq} information on the $NpO_2^+ \cdot UO_2^{2+}$ cation-cation complex is presented in Table 6.1. At $\mu = 6$ M, the LIPAS result of $K_{eq} = 2.4 \pm 0.2$ M^{-1} agrees with both the conventional absorption spectroscopy value of 2.25 ± 0.03 M^{-1} and the Raman value of 2.5 ± 0.5 M^{-1}.

In this thesis a total of five equilibrium constants have been determined, two for the $NpO_2^+ \cdot UO_2^{2+}$ complex, the $NpO_2^+ \cdot Th^{4+}$ complex, the $PuO_2^+ \cdot UO_2^{2+}$ complex, and the $PuO_2^+ \cdot Th^{4+}$ complex. Two of those complexes, the $PuO_2^+ \cdot UO_2^{2+}$ and $PuO_2^+ \cdot Th^{4+}$ complexes, have not been reported previously and involve the PuO_2^+ species, which previously has not had a K_{eq} reported for any complex. Table 6.2 has the K_{eq}, μ,

Table 6.1: Data on K_{eq} and μ for the $NpO_2^+ \cdot UO_2^{2+}$ cation-cation complex.

K_{eq}, M^{-1}	μ, M	Spectroscopy Method†	ref.
≈ 0.6	< 1	L	pw*
0.69 ± 0.01	3.0	S	[5]
2.25 ± 0.03	6.0	S	[20]
2.4 ± 0.2	6	L	pw
2.5 ± 0.5	6.26	R	[12]
3.7 ± 0.1	7	S	[16]

* pw — present work

† — L is LIPAS, S is CAS, and R is Raman spectroscopy.

spectroscopy method, and reference for each K_{eq} determination of a cation-cation complex. In all cases the λ_{max} of the complexed AnO_2^+ species was shifted to a lower wavelength relative to the λ_{max} of the uncomplexed AnO_2^+. The $PuO_2^+ \cdot UO_2^{2+}$ complex shifted by 5.5 nm, the $NpO_2^+ \cdot UO_2^{2+}$ by 4.0 nm at $\mu = 6$ M and by about 1–3 nm at $\mu < 1$ M, and the $NpO_2^+ \cdot Th^{4+}$ by 3.0 nm. The wavelength shifts are slightly larger for the complex containing PuO_2^+ than for the complexes containing NpO_2^+. Because the shifts in this region are to lower wavelengths, the transition being monitored requires more energy to excite; therefore, it is being stabilized. The measured shifts indicate that the PuO_2^+ species is stabilized to a greater extent than the NpO_2^+ species by the complexation. Because these transitions are between non-bonding orbitals on the An atom [46], it is the environment around the An that is being perturbed.

Table 6.2: Updated data on K_{eq} and μ for cation-cation complexes.

Complex	K_{eq}, M^{-1}	μ, M	Spectroscopy Method†	ref.
$UO_2^+ \cdot UO_2^{2+}$	16.1 ± 0.5	2	S	[22]
$NpO_2^+ \cdot Cr^{3+}$	2.62 ± 0.48	8	S	[30]
$NpO_2^+ \cdot Rh^{3+}$	3.31 ± 0.06	8	S	[26]
$NpO_2^+ \cdot Th^{4+}$	1.8 ± 0.9	6	L	pw*
$NpO_2^+ \cdot UO_2^{2+}$	≈ 0.6	< 1	L	pw
	0.69 ± 0.01	3.0	S	[5]
	2.25 ± 0.03	6.0	S	[20]
	2.4 ± 0.2	6	L	pw
	2.5 ± 0.5	6.26	R	[12]
	3.7 ± 0.1	7	S	[16]
$NpO_2^+ \cdot NpO_2^+$	0.82 ± 0.05	4.26	S,R	[12]
	1.41 ± 0.14	6.0	S	[20]
$NpO_2^+ \cdot NpO_2^{2+}$	3.0 ± 0.15	7	S	[16]
$PuO_2^+ \cdot Th^{4+}$	≈ 0.8	6	L	pw
$PuO_2^+ \cdot UO_2^{2+}$	2.2 ± 1.5	6	L	pw
$AmO_2^+ \cdot UO_2^{2+}$	≈ 0.3	4.8	R	[12]
	0.35 ± 0.06	10	S	[17]
$AmO_2^+ \cdot NpO_2^{2+}$	0.095 ± 0.030	S	10	[17]

* pw — present work

† — L is LIPAS, S is CAS, and R is Raman Spectroscopy.

The systematics shown in Fig. 6.1 include the data from the present work. Some trends continue while others do not appear to. The data in Fig. 6.1a of K_{eq} for the $NpO_2^+ \cdot UO_2^{2+}$ complex still increase with increasing μ; it does appear to be approaching some low value for K_{eq} as μ goes to 0. The ionic strength of the solution is an important factor in determining the value of K_{eq} for cation-cation complexes. Increases in μ reduce the amount of H_2O present in the solution and thus reduce the extent to which a species is hydrated. Because Model III is partially dependant upon AnO_2^+ hydration, this result lends credence to this model.

The data in Fig. 6.1b do not appear to maintain the increase in K_{eq} as the effective charge, n, of the ligand cation increases. Whether the down turn at $n = 4$ is due to the differences in μ or is real is difficult to determine without more data. These results are difficult to compare to a model. If the down turn at $n = 4$ is real, it would reduce the credibility of Model I, because a slightly negative charge on the oxygen atom would have a greater attraction for the larger positive charge of a +4 species. Another possible problem could be that the effective charges for the ligands might not be accurate at the higher ionic strengths.

The data in Fig. 6.1c still roughly show a decrease in $\log(K_{eq})$ for the $AnO_2^+ \cdot UO_2^{2+}$ complex as the Z of the AnO_2^+ increases. Again the ionic strengths of the four data points are not the same, but they are the only data available. The identity of the AnO_2^+ species appears to be an important factor in determining the strength of the

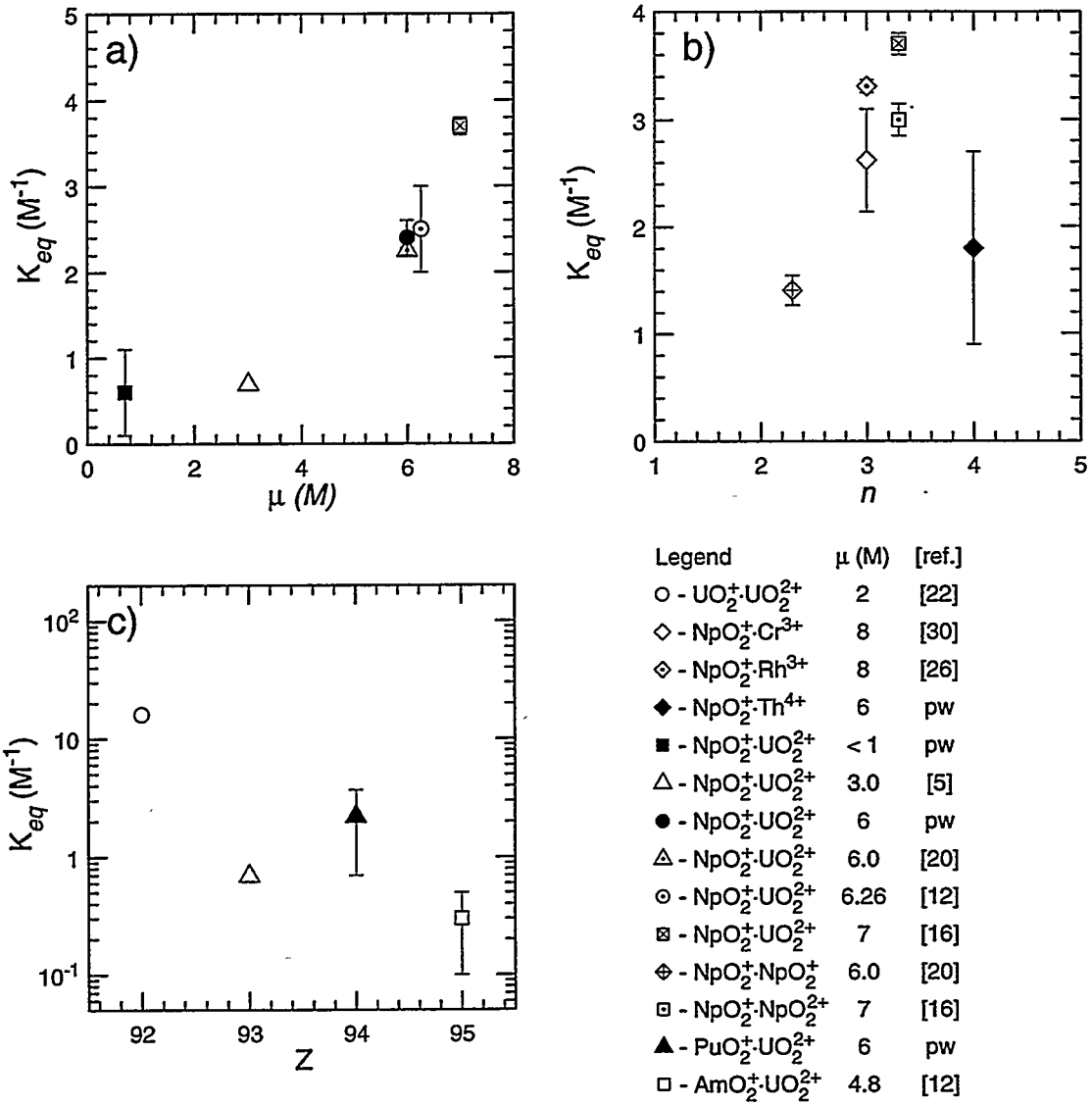

Figure 6.1: Systematics for cation-cation complexes including data from the present work (pw). The data are from Table 6.2; a) K_{eq} for $NpO_2^+ \cdot UO_2^{2+}$ vs. μ; b) K_{eq} for $NpO_2^+ \cdot M^{n+}$ vs. n (effective charge) at approximately constant μ (6–8 M); and c) K_{eq} for $AnO_2^+ \cdot UO_2^{2+}$ vs. Z (atomic number) at approximately constant μ (2–6 M).

complex.

Model I depends upon the formation of a slightly negative charge on the axial oxygens of the AnO_2^+ species. The extent to which the electrons on the oxygen are attracted to the central atom in the AnO_2^+ species is dependent upon its charge. Therefore, an increase in Z would be beneficial; however, an increase in Z also means an increase in the number of electrons shielding this central charge from the oxygen electrons. The net result is a higher Z results in a slightly higher effective charge because the e^- shields the proton almost completely. The data in Fig. 6.1c, which show an inverse proportionality between the $\log(K_{eq})$ and Z, is consistent with this idea and Model I, because the oxygen atoms in the AnO_2^+ cation will have a lower e^- density.

It is difficult to interpret any of the results obtained as being consistent with Model II. The largest deficiency of the model is the absence of AnO_2^+ species forming cation-cation complexes. Model II is used to describe hydrolysis of the AnO_2^{2+} species. Additionally, Model II is the only model that forms outer-sphere complexes while previous results using an inert cation strongly suggest formation of an inner-sphere complex [30].

Model III, the ligand cation in the equatorial plane of the AnO_2^+ cation, is partially dependent on the hydration of the AnO_2^+ cation. Because the magnitude of the cation-cation complex K_{eq} appears to be proportional to the ionic strength of the solution,

this is consistent with the complex formation using Model III. Reducing the amount of water available to form the hydration sphere of the AnO_2^+ allows the ligand cation to compete more effectively with the water to form a complex with the AnO_2^+ species.

6.2 Future

The program SQUAD does not perform the proper error analysis for each data point in the spectra or for molar absorptivities. The LIPAS spectra do not necessarily have constant errors nor are these errors necessarily insignificant. It would be desirable to incorporate into SQUAD the capability to weight each data point with the proper experimental uncertainty rather than treat all points as unweighted.

The main limitation of LIPAS is the small wavelength range that is available for scanning, especially when species like PuO_2^+ which disproportionate, are being studied. The development of Optical Parametric Oscillator (OPO) lasers should alleviate this limitation because OPO lasers scan wavelengths from about 400 nm to 2000 nm without changing dyes which is required by dye lasers. (Harris [47] reviews the early work on tunable OPOs. Laser companies such as LambdaPhysik have recently begun manufacturing OPO lasers.) Coupling this new OPO laser with a LIPAS system should provide a great improvement in the quality of the experimental spectra. A problem that may possibly be encountered is exceeding the region where the PD responds linearly. Because the PD is used for power normalization it is

essential to stay in its linear response region. It would be interesting and useful to use a OPO-LIPAS system to examine several known cation-cation complexes utilizing a much larger wavelength range. This would be exceptionally fruitful for experiments in which the oxidation state is suspected to change.

A review of the experiments on cation-cation complexes indicates that there are seven main variables: the actinide, the ligand metal cation, the ionic strength, the pH, the electrolyte, the temperature, and the solvent. A systematic study involving the alteration of each variable monotonically would give a better understanding of the trends involved and the nature of the interaction. Some potential studies include: (1) studying the various $AnO_2^+ \cdot UO_2^{2+}$ complexes under the same experimental conditions, (2) studying the $NpO_2^+ \cdot M^{n+}$ complexes for a variety of M^{n+} cations under the same experimental conditions (including some studies where the ligand cation concentration is much greater than the AnO_2^+ concentration to look for changes in the ligand cation spectrum), (3) studying the $NpO_2^+ \cdot UO_2^{2+}$ complex at varying ionic strength, pH, or background electrolyte, (4) studying a variety of cation-cation complexes at a variety of temperatures to determine the thermodynamic properties, (5) studying a cation-cation complex like $NpO_2^+ \cdot UO_2^{2+}$ using different solvents (even non-aqueous solvents) to determine how solvent properties like polarity and solvation affect the complex, (6) studying or searching for the various $AnO_2^+ \cdot AnO_2^+$ complexes under defined conditions, and (7) looking for the $PuO_2^+ \cdot NpO_2^+$ complex using high PuO_2^+

concentrations and low NpO_2^+ concentrations (the reverse of the experiment described in Section 5.5).

Better definition of the systematics of cation-cation complexation will provide clues to the form of the complex and the fundamental reason behind its formation. It would be especially useful to determine how the ligand cation spectrum is affected by cation-cation complex formation. The presence of a slight negative charge on the AnO_2^+ oxygen atoms could be validated or the structure of its hydration sphere could be better defined. When analysing the behavior of actinides in high concentration and high ionic strength conditions as a possible waste disposal method, the behavior of "non-run-of-the-mill" complexes like cation-cation complexes might also need to be considered. The formation of AnO_2^+ cation-cation complexes might provide a reason for these AnO_2^+ species to remain stationary under high concentration/high ionic strength conditions or change the conditions where migration might be a problem.

The sensitivity and resolution of LIPAS can be utilized to study actinides in dilute solutions where other forms of absorption spectroscopy are not practical. Plutonium species tend to be insoluble so dilute solutions are unavoidable, especially under environmental conditions. Using a OPO-LIPAS system to analyze a solution containing e.g. plutonium should allow all of the oxidation states that can be stabilized in aqueous solution to be determined simultaneously. Solutions containing several absorbing species should also be possible with a large wavelength range available. The remote

capability of LIPAS allows the atmosphere above the experiment to be controlled and minimizes the possibility on contaminating people or equipment.

Bibliography

[1] Seaborg, G. T.; Loveland, W. D. *The Elements Beyond Uranium*; John Wiley & Sons, New York, 1990.

[2] Katz, J. J.; Seaborg, G. T.; Morss, L. *Chemistry of the Actinide Elements*, 2^{nd} ed.; Chapman and Hall, London, 1986.

[3] Mikheev, N. B.; Spitsyn, V. I.; Kamenskaya, A. N.; Rumer, I. A.; Grozdez, B. A.; Rosenkvich, N. A.; Auerman, L. N. *Dokl. Akad. Nauk SSSR* **1973**, *208*, 1528.

[4] Pyykkö, P. *Chem. Rev.* **1988**, *88*, 563.

[5] Sullivan, J. C.; Hindman, J. C.; Zielen, A. J. *J. Am. Chem. Soc.* **1961**, *83*, 3373.

[6] Pal'shin, E. S.; Myasoedov, B. F.; Davydov, A. V. *Analytical Chemistry of Protactinium*; Ann Arbor-Humphrey Science, Ann Arbor, Michigan, 1970.

[7] Cotton, F. A.; Wilkinson, G. *Advanced Inorganic Chemistry*, 4^{th} ed.; John Wiley & Sons, New York, 1980.

[8] Fuger, J.; Oetting, F. L. *The Chemical Thermodynamics of Actinide Elements and Compounds, Part 2: The Actinide Aqueous Ions*; International Atomic Energy Agency, Vienna, 1976.

[9] Guillaumont, R.; Bouissieres, G.; Muxart, R. *Actinides Rev.* **1968**, *1*, 135.

[10] *Transuranic Elements in the Environment*, Hanson, W. C. Ed.; Technical Information Center, U. S. Department of Energy, Washington D. C., 1980.

[11] Rai, D.; Swanson, J. L. *Nuclear Technology* **1981**, *54*, 107.

[12] Guillaume, B.; Begun, G. M.; Hahn, R. L. *Inorg. Chem.* **1982**, *21*(3), 1159.

[13] Newton, T. W. *J. Phys. Chem.* **1958**, *62*, 943.

[14] Fulton, R. B.; Newton, T. W. *J. Phys. Chem.* **1970**, *74*, 1661.

[15] Newton, T. W. *J. Phys. Chem.* **1959**, *63*, 1493.

[16] Madic, C.; Guillaume, B.; Morisseau, J. C.; Moulin, J. P. *J. Inorg. Nucl. Chem.* **1979**, *41*, 1027.

[17] Guillaume, B.; Hobart, D. E.; Bourges, J. Y. *J. Inorg. Nucl. Chem.* **1981**, *43*, 3295.

[18] Sullivan, J. C.; Zielen, A. J.; Hindman, J. C. *J. Am. Chem. Soc.* **1960**, *82*, 5288.

[19] Hindman, J. C.; Sullivan, J. C.; Cohen, D. *J. Am. Chem. Soc.* **1954**, *76*, 3278.

[20] Stout, B. E.; Choppin, G. R.; Nectoux, F.; Pages, M. *Radiochimica Acta* **1993**, *61*, 65.

[21] Hindman, J. C.; Sullivan, J. C.; Cohen, D. *J. Am. Chem. Soc.* **1958**, *80*, 1812.

[22] Newton, T. W.; Baker, F. B. *Inorg. Chem.* **1965**, *4*(8), 1166.

[23] Sullivan, J. C. *J. Am. Chem. Soc.* **1962**, *84*, 4256.

[24] Baker, F. B.; Newton, T. W.; Kahn, M. *J. Phys. Chem.* **1960**, *64*, 109.

[25] Moore, R. L. *J. Am. Chem. Soc.* **1955**, *77*, 1504.

[26] Murmann, R. K.; Sullivan, J. C. *Inorg. Chem.* **1967**, *6*(5), 892.

[27] Newton, T. W.; Baker, F. B. *J. Phys. Chem.* **1963**, *67*, 1425.

[28] Newton, T. W.; Baker, F. B. *Inorg. Chem.* **1962**, *1*(2), 368.

[29] Newton, T. W.; Burkhart, M. J. *Inorg. Chem.* **1971**, *10*(10), 2323.

[30] Sullivan, J. C. *Inorg. Chem.* **1964**, *3*(3), 315.

[31] Newton, T. W.; Baker, F. B. *J. Phys. Chem.* **1966**, *70*, 1943.

[32] Newton, T. W.; Baker, F. B. *J. Phys. Chem.* **1965**, *69*, 176.

[33] Eigen, M.; Wilkins, R. In *Mechanisms of Inorganic Reactions*; Gould, R. F., Ed.; Advances in Chemistry Series 49; American Chemical Society: Washington, DC, 1965; pp 55-80.

[34] Frolov, A. A.; Rykov, A. G. *J. Inorg. Nucl. Chem.* **1976**, *Supplement*, 61.

[35] Vodovatov, V. A.; Kolokol'sov, V. B.; Kovaleva, T. V.; Mashirov, L. G.; Suglobov, D. N.; Sles', V. G. *Radiokhimiya* **1975**, *17*, 889.

[36] Vodovatov, V. A.; Mashirov, L. G.; Suglobov, D. N. *Radiokhimiya* **1979**, *21*, 830.

[37] Perry, D. L.; Ruben, H.; Templeton, D. H.; Zalkin, A. *Inorg. Chem.* **1980**, *19*, 1067.

[38] Guillaume, B.; Hahn, R. L.; Narten, A. H. *Inorg. Chem.* **1983**, it 22, 109.

[39] Choppin, G. R. *Radiochimica Acta* **1983**, *32*, 43.

[40] Russo, R. E.; Rojas, D.; Roubouch, P.; Silva, R. J. *Rev. Sci. Instrum.* **1990**, *61*, 3729.

[41] Burney, G. A.; Harbour, R. M. *Radiochemisty of Neptunium*; United States Atomic Energy Commission. National Technical Information Service: Springfield, Virginia, 1974; NAS-NS-3060.

[42] Hoffman, D. C. In *Collected Radiochemical and Geochemical Procedures*, 5^{th} ed.; Kleinberg, J., Ed.; United States Department of Energy. Los Alamos National Laboratory: Los Alamos, NM, 1990, I-194; LA-1721.

[43] Riglet, Ch.; Robouch, P.; Vitorge, P. *Radiochemica Acta*, **1989**, *46*, 85.

[44] Cohen, D. *J. Inorg. Nucl. Chem.* **1961**, *18*, 211.

[45] Leggett, D. J. In *Computiational Methods for the Determination of Formation Constants*, Leggett, D. J., Ed.; Plenum Press, New York, 1985, Chapter 6.

[46] Bell, J. T. *J. Inorg. Nucl. Chem.* **1969**, *31*, 703.

[47] Harris, S. E. *Proceeding of the IEEE* **1969**, *57*(12), 2096.